ACLY promotes epidermal regeneration and mitochondrial homeostasis in burn injury by reducing oxidative stress

Shuai Wang[1,2], Jianjun Qi[3], Zunjiang Zhao[2], Junhui Song[1], Dalun Lv[2], Qinglian Xu*[1]

[1]Department of Burns,The First Affiliated Hospital of Anhui Medical University, Hefei, China
[2]Department of Burns and Plastic Surgery,The First Affiliated Hospital of Wannan Medical University (Yijishan Hospital of Wannan Medical University), Wuhu, China
[3]Department of Laboratory Medicine, The First Affiliated Hospital of Wannan Medical University (Yijishan Hospital of Wannan Medical University), Wuhu, Chin

***Corresponding author:**
Qinglian Xu MD, PhD
Department of Burns
The First Affiliated Hospital of Anhui Medical University
Hefei, China
e-mail: yfy128342@fy.ahmu.edu.cn

Submitted: 11 February 2026; **Accepted:** 30 May 2026
Online publication: 4 September 2026

Arch Med Sci 2026
DOI: https://doi.org/10.5114/aoms/222688

Abstract

Introduction: Burn injury causes cellular and metabolic dysfunction associated with mitochondrial damage, oxidative stress and impaired epidermal regeneration, delaying wound healing and raising the risk of chronic complications. As a key metabolic enzyme connecting the tricarboxylic acid cycle (TCA) cycle to lipid synthesis and epigenetic regulation, ATP citrate lyase (ACLY) maintains mitochondrial homeostasis and redox balance, while its role in thermal skin repair remains unclear.

Material and methods: RNA-seq analysis identified molecular changes in thermal injury, while polymerase chain reaction (PCR) and Western blot were used to validate ACLY expression in burn-injured skin tissue. To dissect ACLY function in wound repair, we performed *in vivo* AAV-mediated ACLY knockdown. A panel of assays was also conducted in *in vivo* and *in vitro* ACLY-overexpression models, including hematoxylin and eosin (HE), immunohistochemistry, 5-ethynyl-2′-deoxyuridine (EdU) assay, Transwell migration and invasion, transferase dUTP nick end labelling (TUNEL) staining, acetyl coenzyme A (acetyl-CoA) and ATP quantification, malondialdehyde (MDA) and glutathione (GSH) detection, as well as JC-1 and 2′,7′-dichlorofluorescin diacetate (DCFH-DA) staining.

Results: ACLY expression was markedly downregulated in burn tissues with associated metabolic reprogramming. *In vivo* AAV-mediated ACLY knockdown markedly aggravated burn injury and impaired wound repair. In contrast, ACLY overexpression improved repair outcomes in both *in vivo* and *in vitro* thermal injury models. It relieved oxidative damage by lowering reactive oxygen species (ROS) and MDA, maintained mitochondrial integrity through modulating mitochondrial dynamics, attenuated inflammatory response and cellular apoptosis, and enhanced keratinocyte proliferation as well as migration, ultimately accelerating epidermal regeneration and wound healing.

Conclusions: ACLY plays an important role in regulating mitochondrial stability and epidermal repair following burns. These findings provide novel insights into metabolic mechanisms underlying tissue regeneration and suggest that ACLY may represent a potential therapeutic target for burn healing and regenerative medicine.

Key words: ACLY, burn injury, mitochondrial homeostasis, epidermal regeneration, oxidative stress.

Introduction

Burn injuries are among the most severe and complex traumatic wounds, affecting millions of people worldwide each year [1]. These injuries not only damage local tissue but also trigger systemic physiological disorders [2]. These widespread effects significantly increase the risks of chronic disability, serious medical conditions, and heavy health care costs. The skin serves as the body's main protective barrier, regulating temperature, preventing infections, and maintaining fluid balance [3]. Burn injuries disrupt these vital functions, increasing susceptibility to infections, electrolyte imbalances, and excessive inflammation [4, 5]. Burn injuries initiate systemic pathological changes, including excessive inflammation, oxidative stress, immune dysfunction, and metabolic disturbances [6–8]. A major clinical complication is impaired wound healing, resulting from energy deficiency [9], oxidative damage to cells [10], and persistent tissue injury [11]. Tissue repair requires significant metabolic resources and cellular stability, making the identification of molecular regulators that restore normal function a key goal in burn treatment development.

Mitochondria regulate cellular energy and survival processes that are essential for skin maintenance and wound healing [12, 13]. Burn injuries damage mitochondrial structure and function, causing membrane disruption and impaired energy production [14]. Mitochondrial dysfunction reduces energy production and increases oxidative stress [15]. This damage leads to progressive cell death and inflammation. Keratinocytes, the primary cell type in the skin, rely heavily on functional mitochondria to support key wound healing processes, including cell division, migration, and differentiation [16]. Mitochondrial damage impairs cell survival and tissue repair [17]. While mitochondrial therapies show promise for various injuries, their specific roles in skin regeneration require further investigation.

Among the pathological mechanisms of impaired skin repair caused by mitochondrial injury, dysregulation of the core links in energy metabolism is often the key driving factor [18]. The homeostatic maintenance of intracellular energy metabolism not only depends on the functional integrity of mitochondria but is also closely related to the coordinated regulation of glycolipid metabolism pathways [19]. ATP citrate lyase (ACLY) is a key metabolic enzyme that cleaves citrate to produce two critical metabolites: acetyl coenzyme A (acetyl-CoA) and oxaloacetate [20]. This reaction links catabolic and anabolic pathways while supplying precursors for epigenetic regulation. Studies have suggested that the expression or activity of ACLY often undergoes adaptive changes under metabolic stress or imbalance between the cellular energy supply and demand [21, 22]. The acetyl-CoA generated by ACLY supports lipid synthesis and regulates transcription through histone acetylation, chromatin remodeling, and posttranslational protein modification [23]. Recent studies have identified the diverse functions of ACLY in cancer development, immunometabolism, and cellular responses to nutrient changes. This enzyme may regulate organelle function through protein acetylation, affecting mitochondrial shape, membrane potential, and oxidative stress responses [24]. However, its role in skin repair, particularly in burn conditions characterized by redox imbalance and organelle dysfunction, remains poorly understood.

Based on the above analysis of mitochondrial injury and the core role of ACLY in energy metabolism, we further explored the changes in key metabolic regulators in burn-injured skin tissue through transcriptome sequencing. Transcriptome analysis revealed that ACLY expression was significantly lower in thermally injured skin than in uninjured tissue, suggesting a link between metabolic inhibition and impaired tissue regeneration. These results led to the hypothesis that ACLY may influence the intracellular redox balance and organelle energy metabolism during wound healing. To test this hypothesis, a series of complementary experimental models was established. To study ACLY at the cellular level, immortalized human keratinocytes (HaCaT) and primary mouse epidermal cells were subjected to controlled hyperthermia to simulate burn-induced cellular stress. This model allowed investigation of the effects of ACLY on cell survival, oxidative stress, and mitochondrial function. A comprehensive analysis was performed using multiple techniques, including hematoxylin-eosin staining for tissue structure, terminal deoxynucleotidyl transferase dUTP nick end labelling (TUNEL) for apoptosis, immunohistochemistry for protein localization, reactive oxygen species measurement, mitochondrial membrane potential assessment, and immunoblotting for protein expression. Together, these methods provided insights into the role of ACLY in epidermal repair. Our findings show that increased ACLY expression promotes keratinocyte proliferation and directional migration under thermal stress while reducing oxidative damage and improving mitochondrial balance. This protective effect is associated with changes in mitochondrial dynamics, with increased levels of fusion proteins (mitofusin 1 – MFN1, MFN2, and OPA1) and reduced expression of the fission protein Dynamin-related protein 1 (DRP1). In animal models, ACLY overexpression accelerated burn wound healing, decreased the levels of inflammatory cytokines: interleukin

(IL)-6, tumor necrosis factor α (TNF-α), IL-1β, and interferon γ (IFN-γ); and preserved normal skin structure after thermal injury.

These results identify ACLY lyase as a central metabolic regulator linking organelle function to skin repair after thermal injury. As a key regulator connecting glucose-lipid metabolism and mitochondrial function, ACLY may not only be a critical contributor to energy metabolism imbalance but also exacerbate impaired injury repair by disrupting core repair processes, including cell survival, oxidative stress regulation, and mitochondrial function. Therefore, an in-depth analysis of the specific mechanism of ACLY in postburn skin repair and the clarification of its molecular pathway in regulating mitochondrial energy metabolism in the repair process can provide a novel theoretical basis for elucidating the pathological nature of burn repair disorders. In addition, ACLY is a potential key target for improving burn wound repair and developing targeted treatment strategies and novel interventions for burn management.

Material and methods

Primary mouse keratinocyte and HaCaT cell line culture

Epidermal keratinocytes were isolated from newborn (P1) wild-type mice using standard protocols. The dorsal skin was surgically removed and digested overnight at 4°C in 0.25% trypsin without EDTA. The epidermis was then separated from the dermis and gently dissociated into single cells. The cell suspension was filtered through a 70 µm cell strainer to remove cell clumps and impurities, ensuring high cell purity. The isolated cells were plated in DMEM supplemented with 10% fetal bovine serum and penicillin/streptomycin (100 U/ml) to promote initial attachment. After 4–6 hours of incubation, the culture medium was replaced with serum-free keratinocyte growth medium (K-SFM, Gibco). The primary keratinocytes were maintained under standard conditions (37°C, 5% CO_2, 95% humidity) for 24 hours before the experiments. The HaCaT cell line, obtained from the Chinese Academy of Sciences Cell Repository (accession no. SCSP-5091), was cultured in DMEM (Gibco) supplemented with 10% fetal bovine serum and 1% antibiotic-antimycotic solution. The cells were routinely passaged at 70–80% confluence using 0.25% trypsin-EDTA and maintained in a humidified incubator at 37 °C with 5% CO_2.

Cell treatments and grouping

Cells were divided into four experimental groups to clarify the role of ACLY in heat stress-induced injury: (1) Control group: untreated cells cultured under standard conditions; (2) Heat stress group: cells exposed to 45°C for short (10 minutes) or extended (50 minutes) periods followed by recovery at 37°C; (3) Heat stress + ov-NC group: cells transduced with the empty lentiviral vector (overexpression negative control – NC) and subjected to the same heat stress; (4) Heat stress + ov-ACLY group: cells transduced with the ACLY-overexpression lentivirus and then exposed to heat stress. Lentiviral transduction was conducted 48 hours before heat stress to ensure stable ACLY expression. Cells were collected at 1, 10, and 20 days after treatment for subsequent analyses. To upregulate ACLY expression in cells, the rat ACLY coding sequence (GenBank ID: NM_001111095.1) was cloned into the lentiviral vector pLVX-IRES-ZsGreen1 to construct the overexpression vector pLVX-ACLY-IRES-ZsGreen1. The empty vector served as a negative control (LV-NC). After sequencing verification, the recombinant plasmid was packaged in 293T cells to produce high-titer lentivirus. The viral supernatant was concentrated by ultrafiltration and used to infect HaCaT cells and primary keratinocytes. During infection, virus solution and the polycationic enhancer Polybrene (8 µg/ml) were added [25]. After 18–20 hours, the medium was replaced with fresh culture medium. Zsgreen fluorescence was monitored under a fluorescence microscope at 1, 10, and 20 days post-infection to evaluate transduction efficiency. The mRNA and protein levels of ACLY were determined by quantitative real-time polymerase chain reaction (qPCR) and Western blotting to confirm overexpression efficiency. All experiments were repeated independently at least three times. Negative controls were included for each assay, and data were analyzed by blinded investigators to minimize bias.

Animal treatments and grouping

All animal experiments complied with the Guide for the Care and Use of Laboratory Animals (China NIH) and were approved by the Animal Ethics Committee of The First Affiliated Hospital of Wannan Medical University (approval number: WNMC-AWE-2024412). Male rats were used to reduce the effects of estrogen on inflammation and oxidative stress and to improve the reproducibility of experimental data. Rats were randomly assigned (using computer-generated randomization) to four groups: (1) Control group (n = 5): not subjected to burn injury and injected with sterile PBS (sham-burn control); (2) Burn group (n = 5): subjected to burn injury and injected with sterile PBS [26]; (3) Burn + ov-ACLY group (n = 5): subjected to burn injury followed by local injection of an ACLY-overexpressing lentivirus; (4) Burn + AAV-shACLY group (n = 5): subjected to burn injury followed by local injection of an ACLY-knockdown lentivirus.

To induce *in vivo* ACLY overexpression in wound tissue, a recombinant lentiviral vector (LV002-b, pLenti-GIII-CMV-ACLY-Puro; Applied Biological Materials, Canada) was used for local transduction. The vector expresses rat *Acly* under the CMV promoter and carries a puromycin resistance marker. The viral titer was 1.0×10^8 IU/ml, stored at –80°C. All lentiviral operations were performed in a biosafety level 2 (BSL-2) laboratory following institutional biosafety guidelines. Adult male Sprague-Dawley rats (6–8 weeks old, 200–250 g) were anesthetized with intraperitoneal pentobarbital sodium (40 mg/kg). The dorsal fur was shaved and disinfected with 75% ethanol before burn induction. Thermal injury was induced using a controlled hot-water scalding model. A full-thickness burn was created by exposing a 1.5 cm-diameter area of the dorsal skin to 100°C water for 10 s, whereas control rats underwent the same procedure using room-temperature water. The procedure followed modified methods described by Singer *et al*. and Davenport *et al*. [27, 28]. After injury, the burn area was covered with sterile gauze, and penicillin (40,000 U/day, intramuscular) was administered for 3 consecutive days to prevent infection. Postoperatively, meloxicam (1 mg/kg, subcutaneous) was given for 2 days for analgesia. Rats were housed individually under standard laboratory conditions (temperature 22–25°C, humidity 50–60%, 12-hour light/dark cycle) and monitored daily for general condition, wound status, and food intake. Following burn induction, the virus solution was injected intradermally at four equidistant sites around the wound margin using a 29 G needle. The total injection volume was 100 µl (1×10^8 IU/ml virus diluted in PBS; total virus 1×10^8 IU), with approximately 25 µl per site. Control animals received an equal volume of ov-NC lentivirus solution [29, 30].

At designated time points (days 1, 5, 10, 15, and 20 post-injury), wound healing was photographed using a digital camera, and re-epithelialization rates were quantified using ImageJ according to the formula: ([Original wound size – Remaining wound area] / Original wound size) × 100. Animals were euthanized on days 1, 10, and 20 post-injury/injection with an overdose of pentobarbital sodium. Full-thickness skin (including the wound margin and 3–5 mm of peri-wound tissue) was excised. Two portions of each sample were prepared: one was snap-frozen in liquid nitrogen and stored at –80°C for Western blotting and qPCR; the other was fixed in 10% neutral-buffered formalin for 24–48 hours for HE and immunohistochemical analyses. All analyses were performed by investigators blinded to treatment groups, and experiments were independently repeated to ensure reproducibility.

Reagents and antibodies

The cell culture reagents, including K-SFM, Dulbecco's modified Eagle's medium (DMEM), fetal bovine serum, EDTA-free trypsin (0.25%), and penicillin–streptomycin, were purchased from Gibco (Thermo Fisher Scientific, Waltham, MA, USA). The 2′,7′-dichlorofluorescin diacetate (DCFH-DA) reactive oxygen species (ROS) detection kit and JC-1 mitochondrial membrane potential detection kit were purchased from Beyotime Biotechnology (Shanghai, China). Malondialdehyde (MDA) and glutathione (GSH) assay kits were purchased from Beyotime Biotechnology. The TUNEL apoptosis detection kit was purchased from Beyotime Biotechnology or Roche (Basel, Switzerland). The bicinchoninic acid protein assay kit and enhanced chemiluminescence reagents were purchased from Thermo Fisher Scientific or Millipore (Billerica, MA, USA). Hematoxylin and eosin (HE) staining reagents were obtained from Solarbio (Beijing, China) or Servicebio (Wuhan, China). 4′,6-diamidino-2-phenylindole (DAPI) was purchased from Beyotime Biotechnology. 3,3′-Diaminobenzidine (DAB) staining kits were obtained from ZSGB-BIO (Beijing, China) or Servicebio. The following primary antibodies were used: ACLY (Abcam, cat. no. ab40793); IL-6 (Affinity, cat. no. DF6087); TNF-α (Affinity, cat. no. AF7014); IL-1β (Affinity, cat. no. AF5103); MFN1 (Proteintech, cat. no. 13798-1-AP); MFN2 (Proteintech, cat. no. 12186-1-AP); OPA1 (Proteintech, cat. no. 27733-1-AP); CRMP1 (Proteintech, cat. no. 10317-1-AP); COX IV (Proteintech, cat. no. 11242-1-AP); GAPDH (Abbkine, cat. no. ABL1021); proliferating cell nuclear antigen (PCNA) (Servicebio, cat. no. GB11010); cytokeratin 19 (CK19) (Proteintech, cat. no. 10712-1-AP); IL-17 (Servicebio, cat. no. GB11110); IFN-γ (Affinity, cat. no. DF6045). HRP-conjugated secondary antibodies were purchased from Abbkine (Wuhan, China) and used at 1 : 2000 to 1 : 5000 dilutions. Antigen retrieval was carried out with 10 mM citrate buffer (pH 6.0) before DAB staining.

Hematoxylin and eosin detection

At defined time points after injury (days 1, 5, 10, 15, and 20), skin samples were collected from the wound edges and fixed in 4% paraformaldehyde for 24 hours at room temperature. Fixed tissues were then embedded in paraffin. Five-micrometer-thick sections were cut using a microtome and mounted on slides. Staining began with xylene-based paraffin removal, followed by rehydration through graded ethanol (100%, 95%, 80%, and 70%). Nuclei were stained with 0.5% hematoxylin solution for 5 minutes and rinsed with water, and the cytoplasm was counterstained with 0.5% eosin for 3 minutes. The slides were dehydrated in ethanol (70%, 80%, 95%, and 100%),

cleared with xylene, and permanently mounted with neutral resin under glass coverslips. Histological evaluation was conducted by brightfield microscopy. Epidermal thickness was measured in five randomly selected high-power fields per sample using ImageJ software (NIH). Two blinded reviewers independently assessed keratinocyte proliferation, leukocyte infiltration, and overall tissue structure using both semiquantitative and qualitative criteria.

Immunohistochemistry

The immunohistochemical procedure began with deparaffinization of 5 µm skin sections using xylene, followed by rehydration through a graded alcohol series. Antigen retrieval was performed by heating the slides in 0.01 M citrate buffer (pH 6.0) to near boiling temperature for 15 minutes. To block endogenous peroxidase activity, the sections were treated with 3% hydrogen peroxide for 10 minutes at room temperature. After washing, nonspecific binding was blocked with 5% bovine serum albumin for 30 minutes. The slides were then incubated overnight at 4°C with primary antibodies against PCNA, CK19, IL-17, and IFN-γ, each at a 1 : 200 dilution. Detection was carried out using HRP-conjugated secondary antibodies at 1 : 5000 for 60 minutes at room temperature. Chromogenic staining was performed using DAB, followed by hematoxylin counterstaining of the nuclei. The slides were then cleared with organic solvents and permanently mounted for microscopy. The quantitative analysis included five randomly selected fields at 400× magnification per sample. The DAB-positive area or number of immunoreactive cells was measured using ImageJ -based morphometric analysis.

EdU incorporation assay

Cell proliferation was assessed using a 5-ethynyl-2′-deoxyuridine (EdU) incorporation assay. HaCaT cells and primary murine keratinocytes were seeded in 24-well plates, transfected with ACLY-overexpression or control plasmids, and incubated for 24 hours. Subsequently, cells were exposed to thermal stress (45°C for 10 minutes) and allowed to recover under standard culture conditions for 24 hours. EdU labeling was performed using a commercial EdU Apollo 567 In Vitro Imaging Kit (RiboBio, Guangzhou, China) according to the manufacturer's protocol. Briefly, cells were incubated with 10 µM EdU for 2 hours at 37°C, fixed with 4% paraformaldehyde, and permeabilized with 0.5% Triton X-100. After reaction with the Apollo fluorescent dye, nuclei were counterstained with DAPI. Images were captured using a fluorescence microscope (Leica, Germany), and the percentage of EdU-positive cells (EdU/DAPI ratio) was calculated from at least five randomly selected fields per sample using ImageJ software.

Transwell migration and invasion assays

Cell migratory and invasive capacities were evaluated using Transwell assays. HaCaT cells and primary murine keratinocytes were transfected with ACLY-overexpression or control plasmids and incubated for 24 hours, followed by exposure to thermal stress (45°C for 10 minutes) and recovery for 24 hours under standard conditions. For migration assays, 5×10^4 cells suspended in serum-free medium were seeded into the upper chamber of Transwell inserts (8 µm pore size; Corning, USA). For invasion assays, the upper chambers were pre-coated with Matrigel (BD Biosciences, USA) and seeded with 1×10^5 cells. The lower chambers were filled with complete medium containing 10% FBS as a chemoattractant. After incubation for 24 hours at 37°C, non-migrated cells on the upper membrane surface were removed with a cotton swab, and the migrated or invaded cells on the lower surface were fixed with 4% paraformaldehyde and stained with 0.1% crystal violet. Cells were photographed under a light microscope (Leica, Germany), and the number of migrated or invaded cells was quantified from five randomly selected fields per membrane using ImageJ software.

Wound healing assay

The wound healing assay was performed to evaluate cell migratory ability. HaCaT cells and primary murine keratinocytes were seeded into 6-well plates and cultured to near confluence. Cells were transfected with ACLY-overexpression or control plasmids and incubated for 24 hours, followed by exposure to thermal stress and subsequent recovery for 24 hours. A linear scratch was made across the cell monolayer using a sterile 200–µl pipette tip, and the wells were washed twice with PBS to remove detached cells. Fresh serum-free medium was then added, and images of the wound area were captured at 0 hours and 24 hours using an inverted phase-contrast microscope (Leica, Germany). The wound area was quantified using ImageJ software, and the migration rate was calculated as the percentage of wound closure relative to the initial wound width.

Measurement of acetyl-CoA and ATP levels

Intracellular acetyl-CoA levels were determined using a PicoProbe Acetyl-CoA Assay Kit (Fluorometric, Abcam, ab87546, USA) according to the manufacturer's protocol. Briefly, cells were lysed, deproteinized, and the supernatants were incubated with the reaction mix. Fluorescence inten-

sity was measured at Ex/Em = 535/587 nm using a microplate reader (BioTek, USA). ATP content was measured with an Enhanced ATP Assay Kit (Beyotime Biotechnology, S0027, China), based on a luciferase/luciferin reaction system. Luminescence was detected by a microplate luminometer (Promega, USA). Acetyl-CoA and ATP levels were measured using commercial assay kits. Absolute concentrations were first calculated from standard curves and then normalized to protein content. In this study, cell samples were collected 60 minutes after heat stress to evaluate changes in acetyl-CoA levels. Data are presented as relative values normalized to the control group.

TUNEL assay

Programmed cell death in skin samples was detected using TUNEL staining according to the manufacturer's instructions (Beyotime or Roche). The sections were deparaffinized, rehydrated, and permeabilized with 0.1% Triton X-100 in PBS for 20 minutes. After washing, the slides were incubated with the TUNEL enzyme mixture at 37°C for 60 minutes in a humidified, dark environment. Nuclei were counterstained with DAPI, and samples were mounted with fluorescence-preserving mounting medium. Fluorescence microscopy was used to image five randomly selected fields per sample. Apoptotic cells showed green nuclear fluorescence. The apoptotic rate was calculated as the percentage of TUNEL-positive nuclei relative to total DAPI-stained cells in each field.

Western blotting analysis

Proteins were extracted from tissue samples and cultured keratinocytes using RIPA buffer supplemented with protease and phosphatase inhibitors (Beyotime). After centrifugation, protein concentrations were measured by the bicinchoninic acid assay (Thermo Fisher). For immunoblotting, 20–40 µg of protein was separated on 10–12% SDS-PAGE gels and transferred onto PVDF membranes (Millipore). The membranes were blocked with 5% skim milk in TBST for 60 minutes at room temperature and then incubated overnight at 4°C with primary antibodies against inflammatory cytokines (IL-6, IL-1β, and TNF-α), mitochondrial regulators (MFN1, MFN2, and OPA1), and reference proteins (CRMP1, COX IV, and GAPDH), each diluted 1 : 1000. Detection was performed by incubation with HRP-conjugated secondary antibodies for 60 minutes at room temperature at dilutions ranging from 1 : 2000 to 1 : 5000. For signal detection, enhanced chemiluminescence reagents were used, and the bands were digitally imaged. Densitometric analysis was performed with ImageJ software, and all values were normalized to the corresponding loading control (GAPDH) for quantitative comparison.

Quantitative real-time PCR

RNA was extracted from skin samples and cultured epidermal cells using TRIzol reagent (Invitrogen) following the manufacturer's instructions. The RNA quality was measured by NanoDrop spectrophotometry (Thermo Fisher), and only samples with A260/A280 ratios between 1.8 and 2.0 were used for further analysis. First-strand cDNA synthesis was performed with PrimeScript reverse transcriptase (Takara). Quantitative PCR was conducted using TB Green chemistry (Takara) on StepOnePlus (Applied Biosystems) or CFX96 (Bio-Rad) instruments. The 20 µl reaction mixture contained 10 µl of master mix, 0.4 µl of each forward and reverse primers (10 µM), 2 µl of cDNA template, and 7.2 µl of molecular-grade water. Amplification began with an initial denaturation at 95°C for 30 seconds, followed by 40 cycles of 95°C for 5 seconds and 60°C for 30 seconds. The primers were designed using Primer-BLAST or obtained from published sources. GAPDH was used as the internal reference for normalization. The expression fold changes were calculated by the comparative Ct ($2^{-\Delta\Delta Ct}$) method [31]. All assays included triplicate technical replicates from at least three biological samples.

Transcriptomic and bioinformatics analysis

To investigate the molecular mechanisms underlying thermal injury, RNA sequencing (RNA-seq) was performed on full-thickness skin tissues from control and burn-injured rats. Total RNA was extracted using TRIzol reagent (Invitrogen, USA), and RNA integrity was verified with an Agilent 2100 Bioanalyzer. Samples with RIN ≥ 7.0 were used for library construction with the NEBNext Ultra RNA Library Prep Kit (NEB, USA) and sequenced on an Illumina NovaSeq 6000 platform to generate 150 bp paired-end reads. Clean reads were obtained after quality control with FastQC and Trimmomatic, then aligned to the rat reference genome (Rnor_6.0) using HISAT2. Gene expression was quantified as FPKM values with StringTie, and differentially expressed genes (DEGs) were identified using DESeq2 with the criteria of $|\log_2 FC| \geq 1$ and adjusted $p < 0.05$. Functional enrichment of DEGs was analyzed using ClusterProfiler for GO and KEGG pathways. Mitochondria-related DEGs were extracted based on the GO term "mitochondrion" (GO:0005739) and further analyzed for protein-protein interactions (PPI) using the STRING database (confidence ≥ 0.7), visualized with Cytoscape. Hierarchical clustering and volcano plots were generated with heatmap and ggplot2, re-

spectively, to visualize gene expression patterns between control and burn samples.

MDA and GSH detection

Oxidative stress markers in skin tissues were measured using commercial kits from Nanjing Jiancheng Bioengineering Institute. Fresh skin samples were mechanically homogenized in ice-cold physiological saline and then centrifuged at 2500 × g for 10 minutes at 4°C to collect clear supernatants for analysis. MDA levels were measured by reacting samples with thiobarbituric acid, and the resulting color was quantified at 532 nm using a spectrophotometer. Reduced glutathione was determined using an enzymatic recycling assay with 5,5′-dithiobis-(2-nitrobenzoic acid), and the absorbance was measured at 420 nm. All results were normalized to the total protein content and expressed as nmol of MDA or μg of GSH per mg of tissue protein.

Wound healing observation

Healing dynamics were visually assessed at each time point, with a focus on key wound maturation phases: crust formation, shedding, and new epithelial tissue development. Morphological changes were compared between the experimental groups.

Mitochondrial membrane potential detection using JC-1 staining

Mitochondrial membrane potential was assessed using JC-1 fluorescent dye (Beyotime) following the manufacturer's instructions. Cells and tissue sections were incubated with JC-1 solution at 37°C for 20 minutes in the dark. After two washes with buffer, the samples were immediately examined by fluorescence microscopy. JC-1 displays distinct fluorescence: red signals indicate intact mitochondrial membrane potential ($\Delta\Psi m$) through J-aggregate formation, whereas green signals reflect monomeric JC-1 accumulation associated with membrane depolarization. Mitochondrial membrane potential was quantified by calculating the red-to-green fluorescence emission ratio using digital image analysis (ImageJ, NIH). Higher ratios indicate better mitochondrial integrity.

Intracellular ROS detection using DCFH-DA staining

Cellular oxidative stress was measured using a DCFH-DA fluorescence detection system (Beyotime). Keratinocyte cultures or frozen tissue sections were incubated with 10 μM DCFH-DA at 37°C for 30 minutes in the dark. After incubation, the unbound probe was removed by three PBS washes. Fluorescence was captured using an inverted microscope with FITC settings (excitation, 488 nm; emission, 525 nm). Quantitative analysis was performed using ImageJ software to measure the average pixel intensity from randomly selected microscopic fields, which reflects the reactive oxygen species levels. Each condition was tested in triplicate to ensure data reliability.

Statistical analysis

All quantitative data were analyzed using IBM SPSS Statistics version 19 (IBM Corp., Armonk, NY, USA) with investigators blinded to experimental conditions during analysis. Results are expressed as arithmetic mean ± SEM. Normally distributed data involving multiple groups were analyzed using two-way analysis of variance (ANOVA) followed by Tukey's multiple-comparison test. Non-normally distributed variables were assessed using the Mann-Whitney *U* test. Statistical significance thresholds were established as: $^{*}p < 0.05$, $^{**}p < 0.01$, $^{***}p < 0.001$ vs. the control group; $\#p < 0.05$, $\#\#p < 0.01$, $\#\#\#p < 0.001$ vs. the heat stress + ov-NC group.

Results

ACLY was identified as a key gene downregulated in burn-induced skin injury and heat-stressed keratinocytes

To investigate the molecular mechanisms of thermal injury, transcriptomic profiling was performed on skin tissues from control and burned rats. First, we characterized the global gene expression changes using a heatmap (Figure 1A) and volcano plot (Figure 1B), revealing widespread differential gene expression between the two groups. Given the known role of mitochondrial dysfunction in stress-induced tissue damage, we intersected these differentially expressed genes (DEGs) with the MitoCarta database, yielding 73 mitochondria-related candidate genes (Figure 1C). To explore the functional implications of these candidates, we conducted KEGG pathway enrichment analysis. The results indicated that these genes were predominantly enriched in metabolic pathways and fatty acid metabolism (Figure 1D, E), suggesting that dysregulation of fatty acid metabolism is a core feature of burn-induced skin injury. Next, we constructed a protein-protein interaction network and ranked genes by their degree of connectivity to identify hub genes within the fatty acid metabolism pathway. The top 10 hub genes are presented in Figure 1F, with *FASN* emerging as the gene with the highest degree value, while *ACLY* also showed high connectivity. To validate these findings, we first performed qPCR analysis on the top 10 hub genes using skin tissues from the *in vivo* burn model (Supplementa-

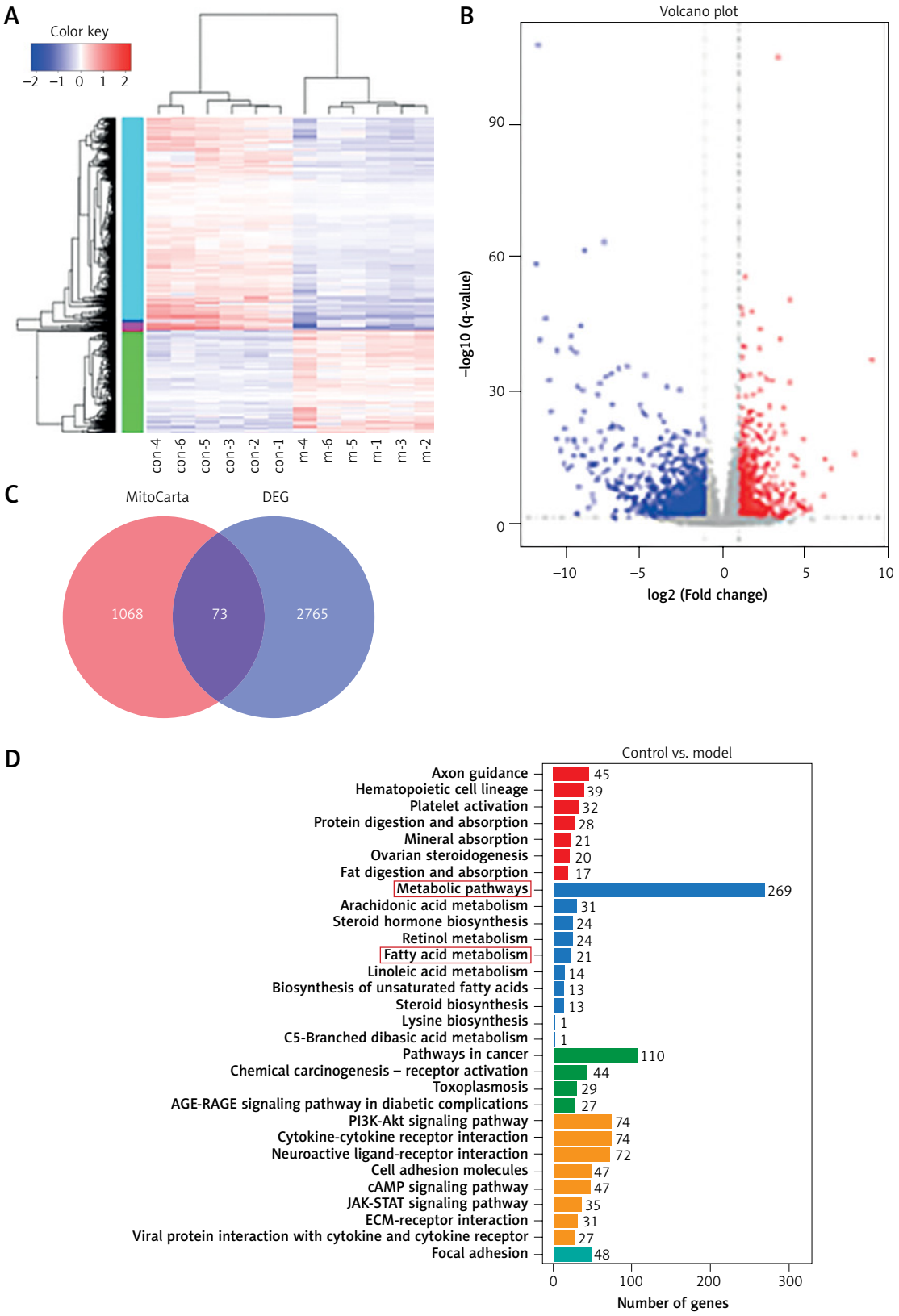

Figure 1. Transcriptomic profiling and identification of ACLY in thermally injured skin. **A** – Heatmap of gene expression patterns in control and burned rat skin. **B** –Volcano plot showing differentially expressed genes (DEGs) between control and burned skin. **C** – Venn diagram showing the overlap between DEGs and mitochondria-related genes (n = 73). **D** – KEGG enrichment of the 73 DEGs, highlighting metabolic pathways and fatty acid metabolism

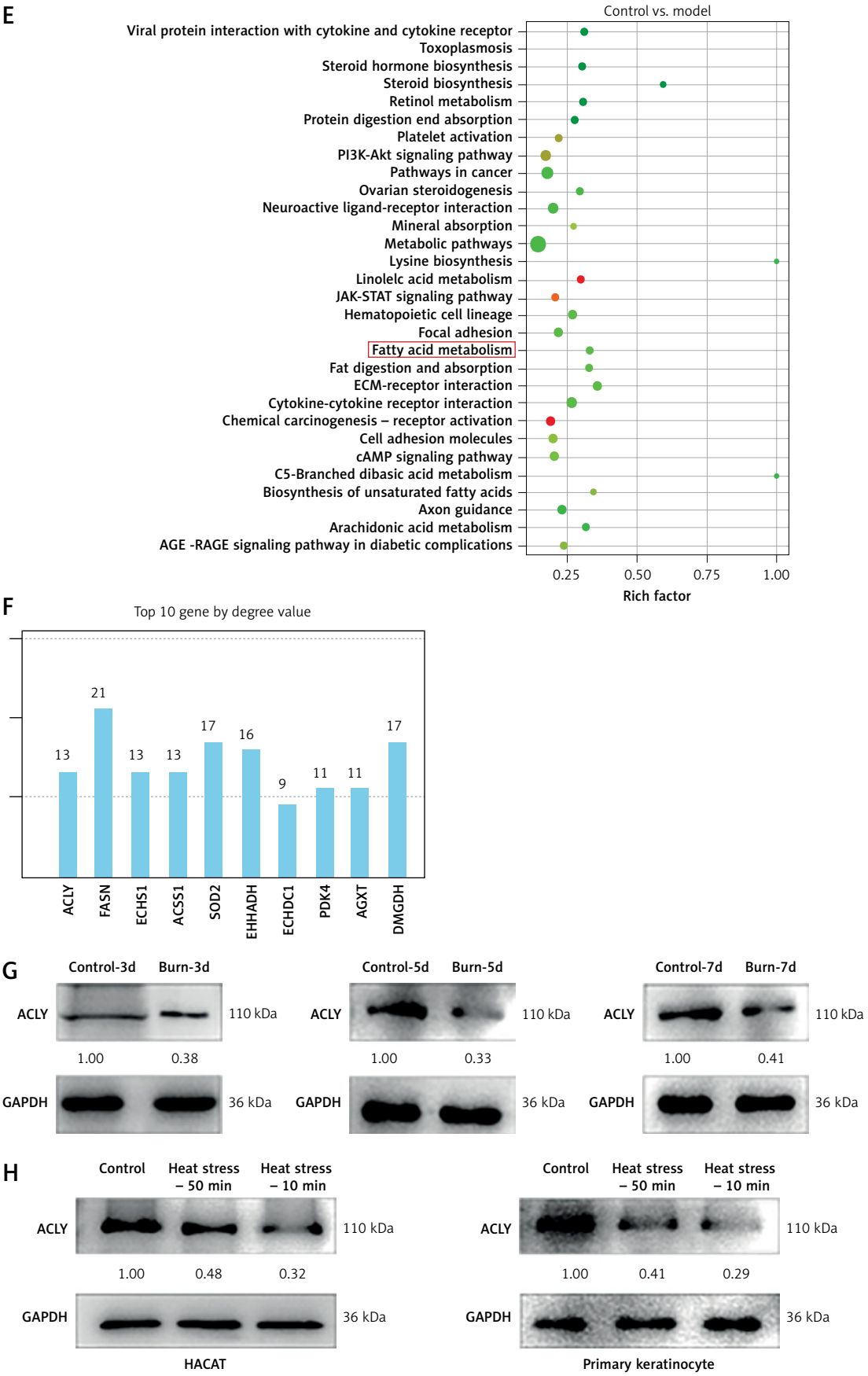

Figure 1. Cont. **E** – KEGG enrichment of the 73 DEGs, highlighting metabolic pathways and fatty acid metabolism. **F** – Top 10 hub genes ranked by PPI degree value, with ACLY as the leading hub. **G** – Western blot of ACLY in rat skin at 3, 5, and 7 days after burn injury. **H** – ACLY protein levels in heat-stressed HaCaT cells and primary keratinocytes. GAPDH was used as the loading control

ry Figure S1A). *ACLY* and *FASN* showed consistent downregulation in the burn group across all time points (days 3, 5, and 7). We then verified the expression changes at the protein level via Western blot. As shown in Figure 1G, ACLY protein levels were significantly and consistently downregulated in burned rat skin at days 3, 5, and 7 post-injury. This finding was further replicated in two independent *in vitro* heat stress models (HaCaT cells and primary keratinocytes, Figure 1H), confirming a robust reduction in ACLY protein expression under heat stress. In contrast, although *FASN* mRNA was downregulated in the burn model, its protein level did not show consistent or significant changes under heat stress in primary keratinocytes (Supplementary Figure S1B).

Given that ACLY exhibited consistent, multi-level downregulation (transcriptomic, mRNA, and protein levels) across both *in vivo* and *in vitro* models, we prioritized ACLY as the key target gene for subsequent functional investigations.

ACLY knockdown *in vivo* and ACLY-mediated promotion of keratinocyte proliferation, migration and invasion under heat stress *in vitro*

To further validate the functional role of ACLY in burn-induced skin injury, we conducted complementary loss-of-function experiments using AAV-mediated ACLY knockdown (Burn + AAV-shACLY) *in vivo*. As shown in Supplementary Figure S2A, ACLY knockdown significantly aggravated burn wound progression at both days 1 and 20 post-injury, resulting in larger necrotic areas and delayed wound closure compared with the burn group. HE staining further confirmed that ACLY inhibition impaired epidermal regeneration and increased tissue destruction (Supplementary Figure S2B). Mechanistically, ACLY knockdown exacerbated burn-induced cell apoptosis, as demonstrated by increased TUNEL-positive cells (Supplementary Figure S2C), while suppressing cell proliferation, as evidenced by reduced PCNA expression (Supplementary Figure S2D). Additionally, ACLY inhibition amplified the local inflammatory response, with significantly elevated IL-17 expression in the burn wound microenvironment (Supplementary Figure S2E). Consistent with these findings, ACLY knockdown further aggravated oxidative stress, as shown by enhanced ROS production (Figure S2F), elevated MDA levels, and decreased GSH levels (Supplementary Figure S2G, H). JC-1 staining further revealed that ACLY inhibition worsened burn-induced mitochondrial membrane potential depolarization, indicating more severe mitochondrial dysfunction (Supplementary Figure S2I). Collectively, these loss-of-function results complement our gain-of-function data, supporting a protective role for ACLY in burn wound repair.

Consistent with these in vivo findings, we validated the efficiency of our ACLY overexpression system *in vitro*. Immunoblotting verified increased ACLY protein levels following lentiviral transduction (Figure 2A), and qPCR confirmed robust ACLY mRNA overexpression in HaCaT and primary murine keratinocytes (Figure 2B, C). Functional assays showed that cells transduced with the ACLY-overexpressing lentivirus and then subjected to thermal stress exhibited improved keratinocyte responses. EdU incorporation revealed that DNA synthesis was strongly suppressed by heat ex-

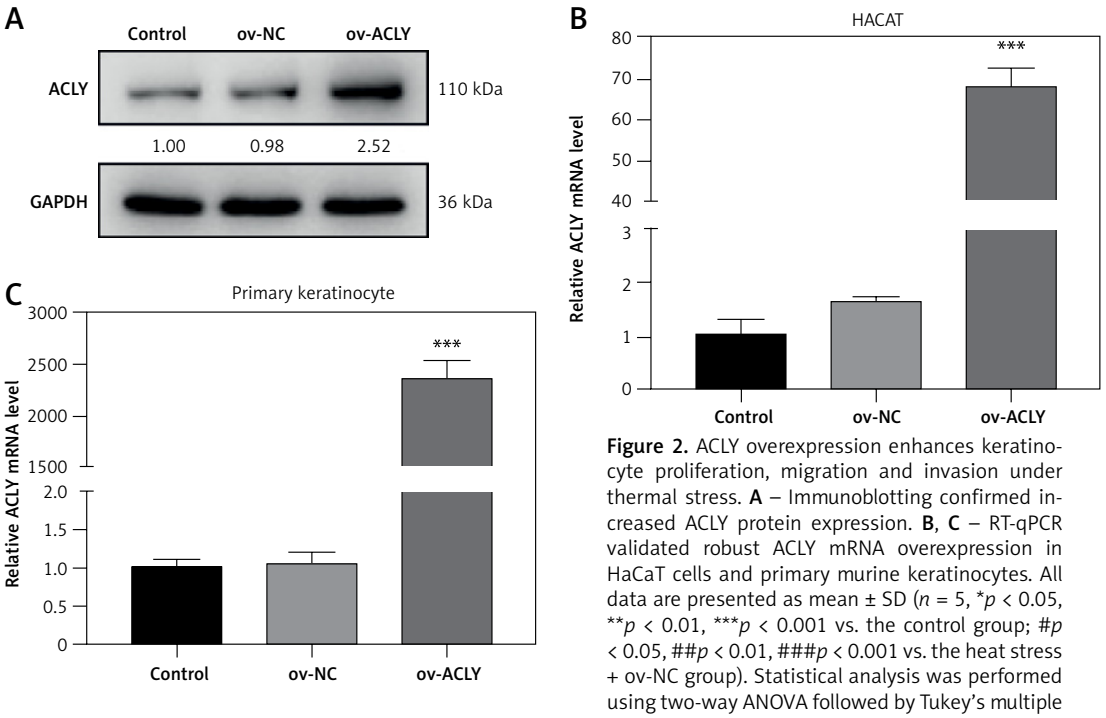

Figure 2. ACLY overexpression enhances keratinocyte proliferation, migration and invasion under thermal stress. **A** – Immunoblotting confirmed increased ACLY protein expression. **B**, **C** – RT-qPCR validated robust ACLY mRNA overexpression in HaCaT cells and primary murine keratinocytes. All data are presented as mean ± SD (n = 5, $^{*}p < 0.05$, $^{**}p < 0.01$, $^{***}p < 0.001$ vs. the control group; #$p < 0.05$, ##$p < 0.01$, ###$p < 0.001$ vs. the heat stress + ov-NC group). Statistical analysis was performed using two-way ANOVA followed by Tukey's multiple comparison test

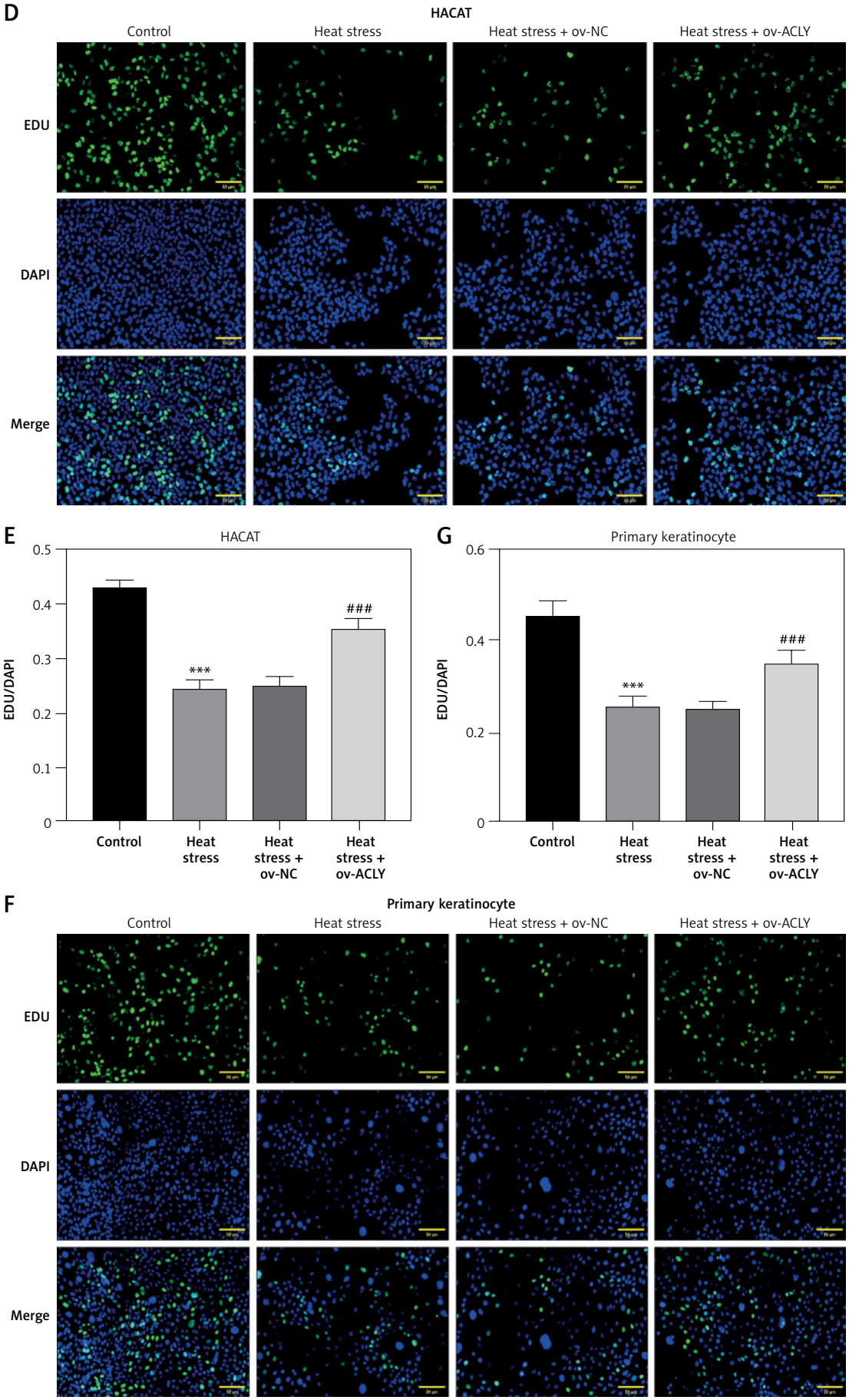

Figure 2. Cont. **D–F** – Representative EdU incorporation images in HaCaT and primary keratinocytes. **E–G** – Quantification of EdU/DAPI ratios showing that ACLY overexpression rescued heat-induced suppression of DNA synthesis. All data are presented as mean ± SD (n = 5, *p < 0.05, **p < 0.01, ***p < 0.001 vs. the control group; #p < 0.05, ##p < 0.01, ###p < 0.001 vs. the heat stress + ov-NC group). Statistical analysis was performed using two-way ANOVA followed by Tukey's multiple comparison test

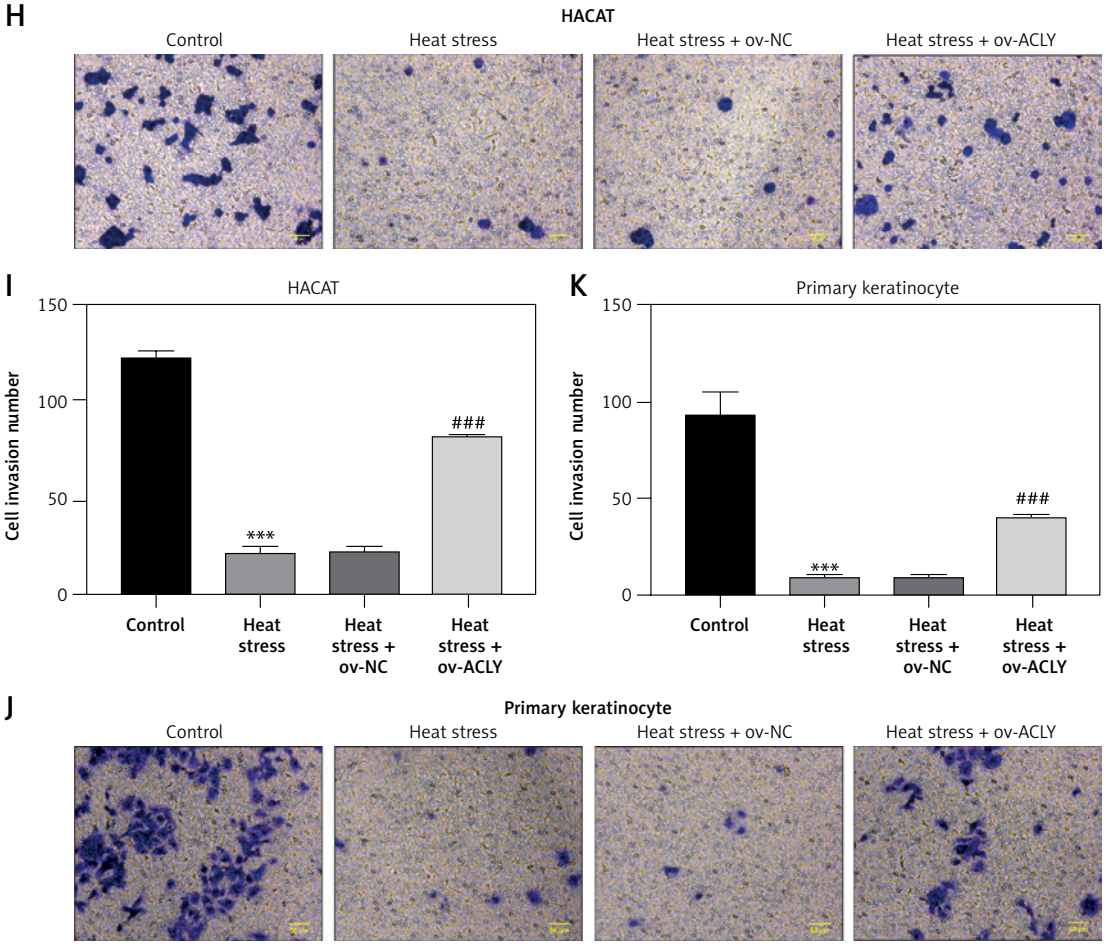

Figure 2. Cont. **H–J** – Representative Transwell images demonstrating improved migration and invasion in ACLY-overexpressing HaCaT cells and primary keratinocytes under heat stress. **I–K** – Quantitative analyses of cell migration and invasion. All data are presented as mean ± SD (n = 5, *p < 0.05, **p < 0.01, ***p < 0.001 vs. the control group; #p < 0.05, ##p < 0.01, ###p < 0.001 vs. the heat stress + ov-NC group). Statistical analysis was performed using two-way ANOVA followed by Tukey's multiple comparison test

posure but significantly restored in ACLY-overexpressing cells; representative EdU images for HaCaT and primary keratinocytes are shown in Figure 2D and F, respectively, with quantitative EdU/DAPI ratios presented in Figure 2E and Figure 2G. Transwell assays indicated that thermal stress impaired both migration and invasive capacity, whereas ACLY-overexpressing cells displayed markedly enhanced migratory and invasive capacities. Representative images for HaCaT and primary keratinocyte assays are shown in Figure 2H and Figure 2J, with the corresponding quantifications in Figure 2I and K. Collectively, these data indicate that ACLY overexpression attenuated heat-induced defects in keratinocyte proliferation and invasion, supporting its role in promoting epidermal regeneration after burn injury. To investigate the role of ACLY in thermal stress adaptation, HaCaT cells and primary murine keratinocytes were first transfected with control (ov-NC) or ACLY-overexpressing (ov-ACLY) vectors and then exposed to 45°C for 10 minutes. CCK-8 assays revealed significant thermal cytotoxicity in both cell types, which was partially alleviated by pre-transfection-mediated ACLY overexpression (Supplementary Figure S3A, B). Thermal stress also impaired cell migration, as shown by wound-closure assays: representative wound images for HaCaT and primary keratinocytes are shown in Supplementary Figure S3C and E, respectively, and the corresponding quantitative analyses of wound closure for HaCaT and primary keratinocytes are presented in Supplementary Figure S3D and F, respectively. Together, these supplementary results provide further evidence that ACLY overexpression prior to heat exposure mitigates heat-induced cytotoxicity and facilitates recovery of keratinocyte migratory function.

ACLY overexpression alleviates oxidative stress and maintains mitochondrial function under heat stress

To evaluate the impact of ACLY on oxidative balance, intracellular ROS levels were measured

using DCFH-DA staining. Heat stress markedly elevated ROS accumulation in HaCaT cells and primary keratinocytes, whereas ACLY overexpression significantly attenuated this increase (Figure 3A–C), indicating reduced oxidative stress. JC-1 staining further revealed that thermal stress induced mitochondrial depolarization, as evidenced by a reduced red/green fluorescence ratio. Notably, ACLY attenuated the reduction in mitochondrial membrane potential ($\Delta\Psi m$) in both HaCaT and primary keratinocytes, suggesting a protective effect on mitochondrial membrane potential preservation (Figure 3D–F). Consistently, qPCR analysis showed that heat stress suppressed the transcription of mitochondrial fusion genes (MFN1, MFN2, OPA1) while upregulating the fission gene DRP1 in both HaCaT and primary keratinocytes. Importantly, ACLY overexpression reversed these transcriptional changes, restoring the balance between fusion and fission marker expression at the mRNA level (Figure 3G, H). Western blotting analysis demonstrated that heat stress disrupted mitochondrial dynamics by decreasing the expression of fusion-related proteins (MFN1, MFN2, OPA1) and elevating the fission marker DRP1. These alterations were reversed following ACLY overexpression (Figure 3I). Collectively, these findings indicate that ACLY may protect keratinocytes from heat-induced injury by reducing oxidative stress, increasing mitochondrial membrane potential, and restoring mitochondrial dynamics. In addition, biochemical assays showed that heat stress significantly reduced the levels of reduced glutathione (GSH) in HaCaT cells (Supplementary Figure S4A), with a similar decrease observed in primary keratinocytes (Supplementary Figure S4B). Meanwhile, heat stress increased lipid peroxidation products (MDA) in both HaCaT and primary murine keratinocytes (Supplementary Figure S4C, D). Moreover, ACLY overexpression was associated with increased cellular acetyl-CoA levels in HaCaT and primary keratinocytes (Supplementary Figure S4E, F) and enhanced ATP production in both cell types (Supplementary Figure S4G, H). TUNEL staining further demonstrated that heat stress markedly induced apoptosis (Supplementary Fig-

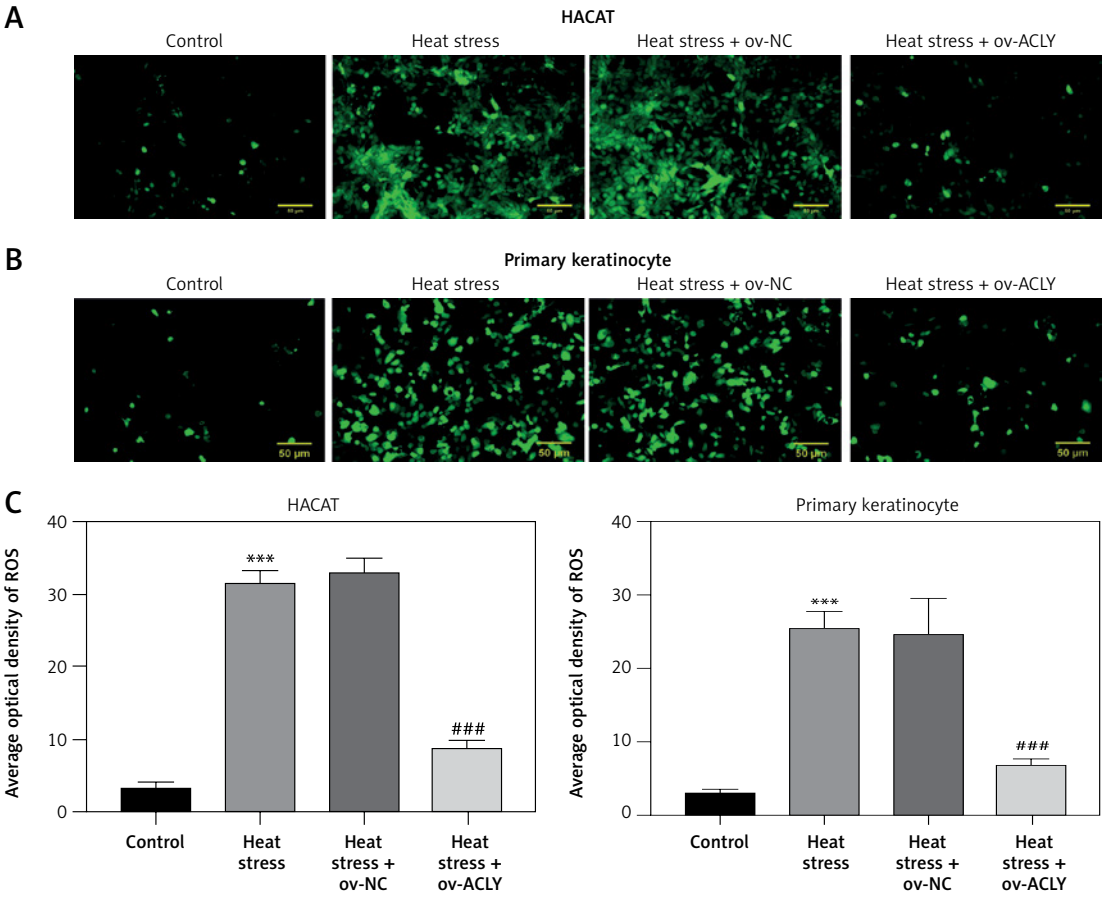

Figure 3. ACLY attenuates oxidative stress and preserves mitochondrial homeostasis under heat stress. **A**, **B** – Representative fluorescence images of DCFH-DA staining showing ROS levels in HaCaT cells (A) and primary keratinocytes (**B**) under the indicated conditions. Scale bars, 50 μm. **C** – Quantification of intracellular ROS fluorescence intensity. All data are presented as mean ± SD (n = 5, *p < 0.05, **p < 0.01, ***p < 0.001 vs. the control group; #p < 0.05, ##p < 0.01, ###p < 0.001 vs. the heat stress + ov-NC group). Statistical analysis was performed using two-way ANOVA followed by Tukey's multiple comparison test

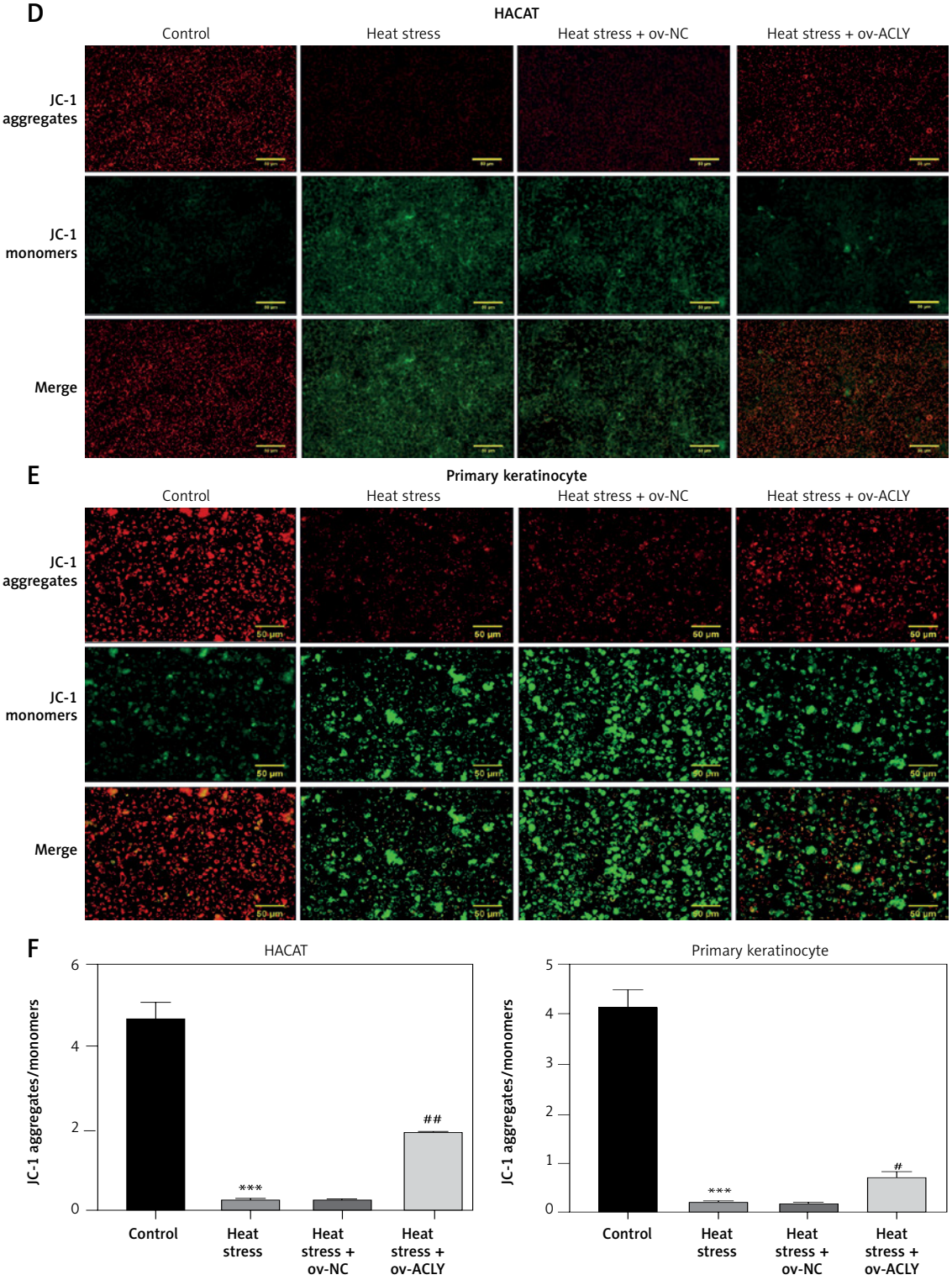

Figure 3. Cont. **D**, **E** – JC-1 staining showing mitochondrial membrane potential (ΔΨm) in HaCaT (**D**) and primary keratinocytes (**E**). Scale bars, 50 μm. **F** – Quantification of the red/green fluorescence intensity ratio. All data are presented as mean ± SD (n = 5, *p < 0.05, **p < 0.01, ***p < 0.001 vs. the control group; #p < 0.05, ##p < 0.01, ###p < 0.001 vs. the heat stress + ov-NC group). Statistical analysis was performed using two-way ANOVA followed by Tukey's multiple comparison test

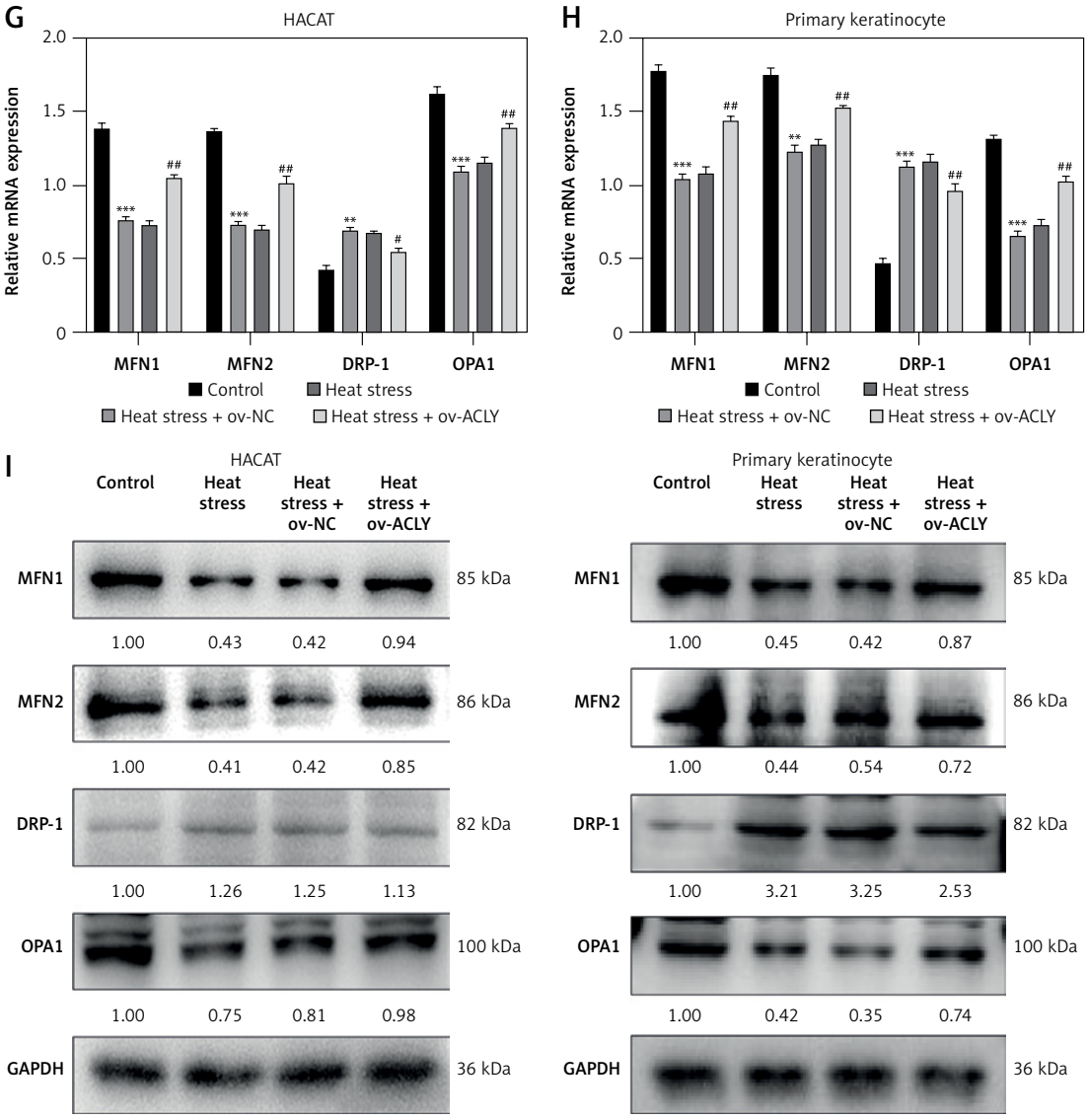

Figure 3. Cont. **G**, **H** – qPCR analysis of mitochondrial dynamics-related genes (MFN1, MFN2, OPA1, and DRP1) in HaCaT (**G**) and primary keratinocytes (**H**). **I** – Western blot analysis of MFN1, MFN2, OPA1, and DRP1 protein levels in HaCaT and primary keratinocytes. GAPDH served as the loading control. All data are presented as mean ± SD (n = 5, *p < 0.05, **p < 0.01, ***p < 0.001 vs. the control group; #p < 0.05, ##p < 0.01, ###p < 0.001 vs. the heat stress + ov-NC group). Statistical analysis was performed using two-way ANOVA followed by Tukey's multiple comparison test

ure S4I, K), whereas ACLY overexpression substantially reduced the number of TUNEL-positive cells; quantitative analysis confirmed this effect in both HaCaT (Supplementary Figure S4J) and primary keratinocytes (Supplementary Figure S4L).

ACLY promotes epidermal proliferation and regeneration while reducing apoptosis in burn-injured skin

To investigate the role of ACLY in postburn re-epithelialization, we analyzed proliferation and progenitor marker levels by immunohistochemistry. Compared with those in uninjured control tissues, proliferating cell nuclear antigen (PCNA) levels were significantly lower in burn-injured tissues at days 1, 10, and 20 after injury. ACLY-overexpressing tissues presented partial restoration of this proliferation marker (Figure 4A). Parallel analysis of CK19, a marker of epithelial progenitor cells, revealed similar trends. Thermal injury significantly reduced CK19 expression, which was notably improved by ACLY overexpression (Figure 4B). Apoptosis assessment using TUNEL revealed increased DNA fragmentation in burned tissues at all time points, indicating elevated programmed cell death. This increase was significantly reduced in ACLY-overexpressing animals (Figure 4C, E, G). The same is true for the quantitative evaluation of cell apoptosis by TUNEL method at 1 day,

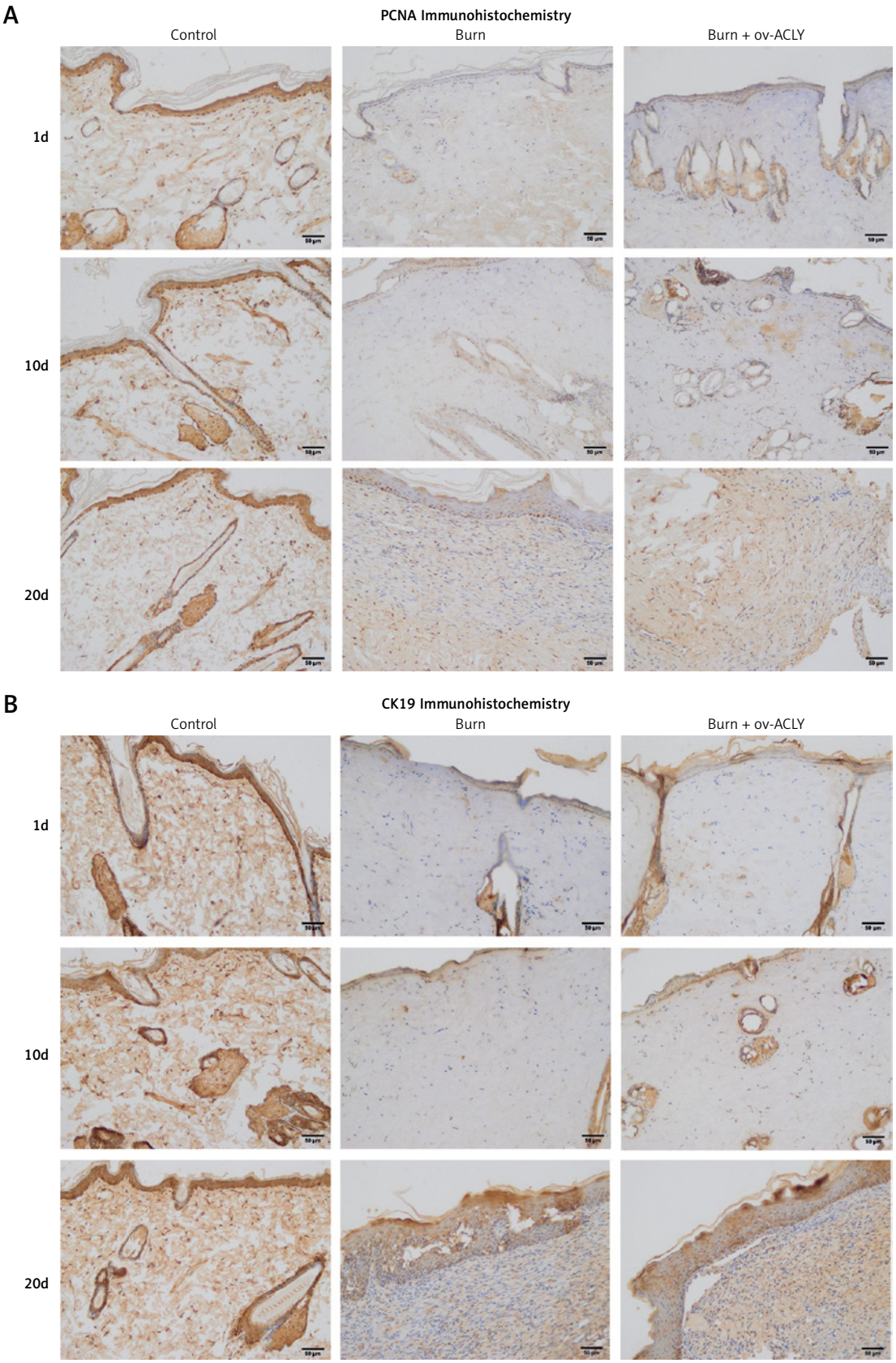

Figure 4. ACLY overexpression promotes epidermal proliferation, reduces apoptosis, and enhances regeneration during skin burn wound healing. **A** – Immunohistochemical staining of PCNA in skin sections at days 1, 10, and 20 postburn. Burn injury markedly reduced PCNA expression compared with uninjured controls, whereas ACLY overexpression partially restored this proliferation marker. **B** – Immunohistochemical staining of CK19, a marker of epithelial progenitor cells, showing similar trends. Burn injury significantly decreased CK19 expression, which was partially restored by ACLY overexpression. All data are presented as mean ± SD (n = 5, *p < 0.05, **p < 0.01, ***p < 0.001 vs. the control group; #p < 0.05, ##p < 0.01, ###p < 0.001 vs. the burn group). Statistical analysis was performed using two-way ANOVA followed by Tukey's multiple comparison test

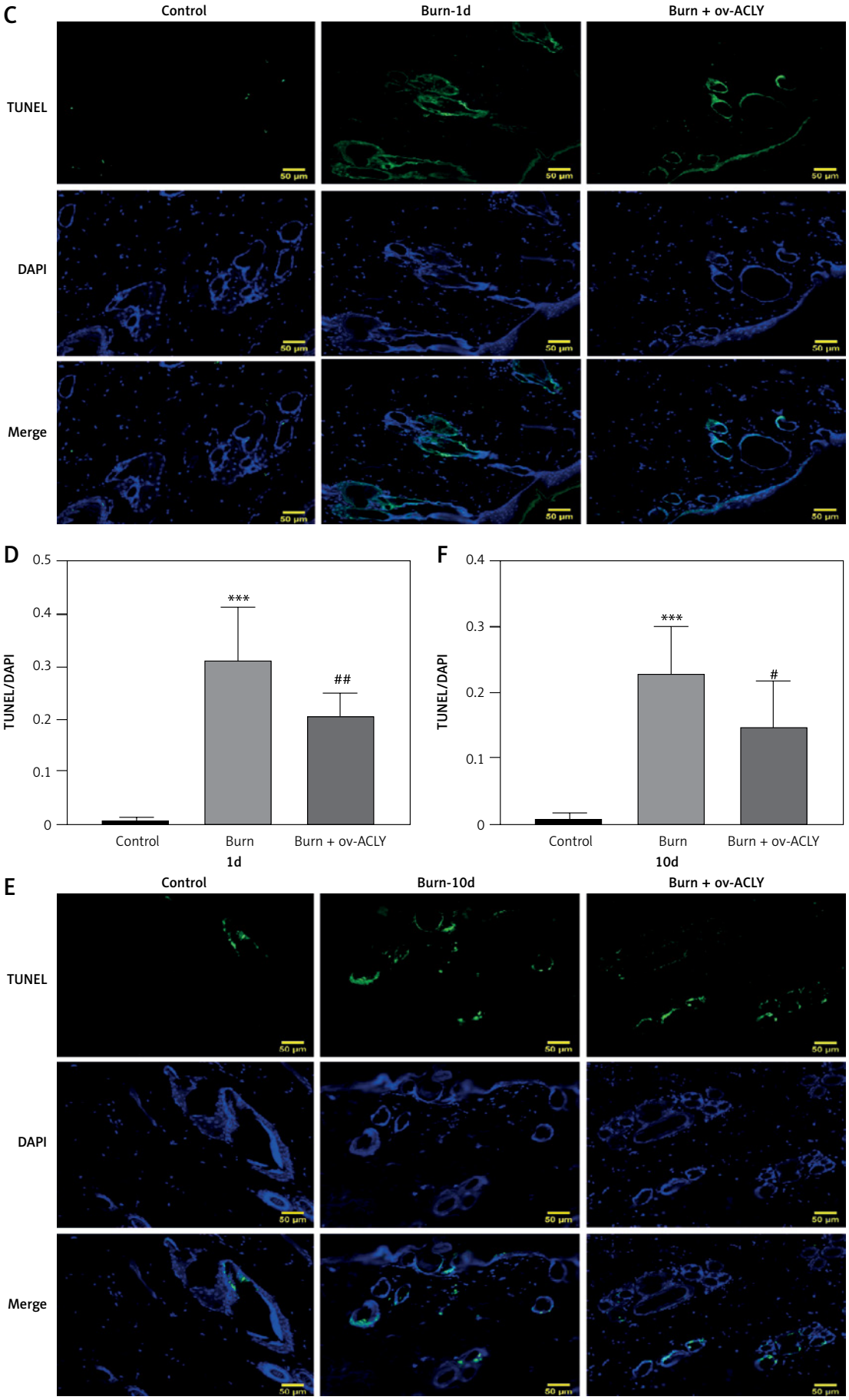

Figure 4. Cont. **C**, **E**, **G** – Representative TUNEL staining images showing apoptosis in burn-injured skin at 1 day (**C**), 10 days (**E**), and 20 days (**G**). Burn injury induced DNA fragmentation, while ACLY overexpression reduced TUNEL-positive cells. **D**, **F**, **H** – Quantitative analysis of TUNEL-positive cells at 1 day (**D**), 10 days (**F**), and 20 days (**H**). ACLY overexpression significantly decreased apoptosis at all examined time points. All data are presented as mean ± SD (n = 5, *p < 0.05, **p < 0.01, ***p < 0.001 vs. the control group; #p < 0.05, ##p < 0.01, ###p < 0.001 vs. the burn group). Statistical analysis was performed using two-way ANOVA followed by Tukey's multiple comparison test

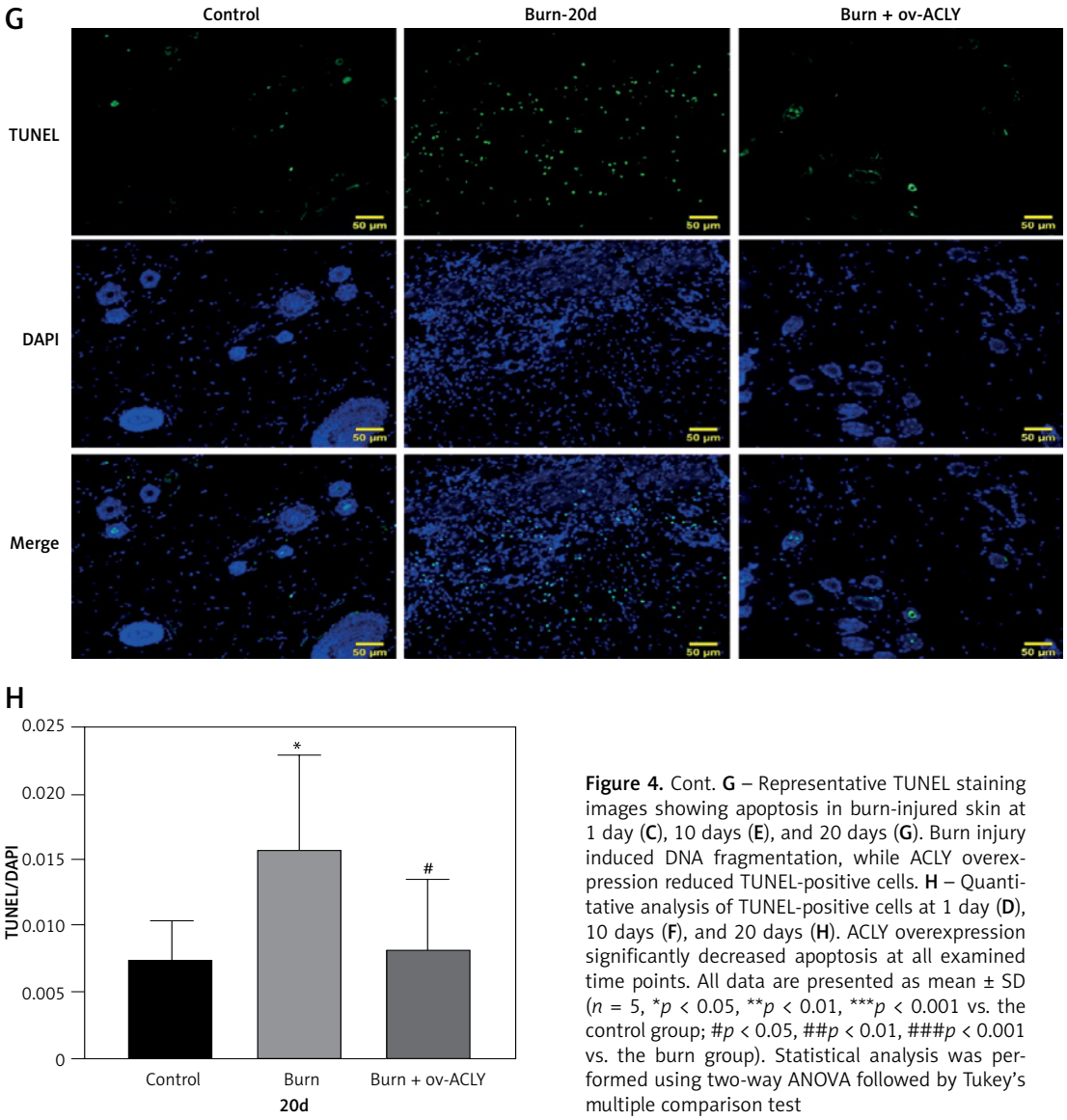

Figure 4. Cont. **G** – Representative TUNEL staining images showing apoptosis in burn-injured skin at 1 day (**C**), 10 days (**E**), and 20 days (**G**). Burn injury induced DNA fragmentation, while ACLY overexpression reduced TUNEL-positive cells. **H** – Quantitative analysis of TUNEL-positive cells at 1 day (**D**), 10 days (**F**), and 20 days (**H**). ACLY overexpression significantly decreased apoptosis at all examined time points. All data are presented as mean ± SD (n = 5, *p < 0.05, **p < 0.01, ***p < 0.001 vs. the control group; #p < 0.05, ##p < 0.01, ###p < 0.001 vs. the burn group). Statistical analysis was performed using two-way ANOVA followed by Tukey's multiple comparison test

10 days, and 20 days (Figure 4D, F, H). These results indicate that ACLY is associated with enhanced epidermal repair by promoting proliferation-associated marker expression and reducing apoptosis during wound healing.

ACLY overexpression alleviates oxidative stress and mitochondrial alterations in burned skin tissue

To further investigate the role of ACLY in redox balance and mitochondrial function following thermal injury, we first examined ROS accumulation by DCFH-DA staining. Burned tissues displayed markedly increased ROS signals at days 1, 10, and 20 compared with control skin, whereas ACLY overexpression significantly reduced ROS accumulation (Figure 5A). Consistently, biochemical assays revealed that burn injury elevated lipid peroxidation, as indicated by increased MDA levels, and depleted the antioxidant GSH pool. These alterations were partially reversed in ACLY-overexpressing animals (Figure 5B). We next assessed mitochondrial membrane potential ($\Delta\Psi$m) by JC-1 staining. Burned tissues exhibited a progressive decline in $\Delta\Psi$m at days 1, 10, and 20, manifested by a lower red/green fluorescence ratio. In contrast, ACLY overexpression attenuated the loss of mitochondrial potential across all time points (Figure 5C, E, G). To further explore mitochondrial dynamics, we analyzed the expression of fusion- and fission-related proteins. Western blotting demonstrated that burn injury markedly reduced MFN1, MFN2, and OPA1 while increasing DRP1. These imbalances were reversed upon ACLY overexpression (Figure 5D, F, H). Collectively, these findings indicate that ACLY may protect against burn-induced oxidative damage and is associated with preservation of redox balance, mitochondrial

membrane potential, and mitochondrial dynamics-related protein expression.

ACLY promotes burn wound healing and attenuates tissue inflammation

Macroscopic observation revealed that control wounds healed rapidly, while burn injuries showed severe necrosis and delayed closure throughout the 20-day observation period. In contrast, ACLY overexpression accelerated eschar detachment and improved wound closure (Figure 6A). Quantitative analysis confirmed significantly accelerated healing in ACLY-overexpressing animals compared with untreated burn wounds, particularly

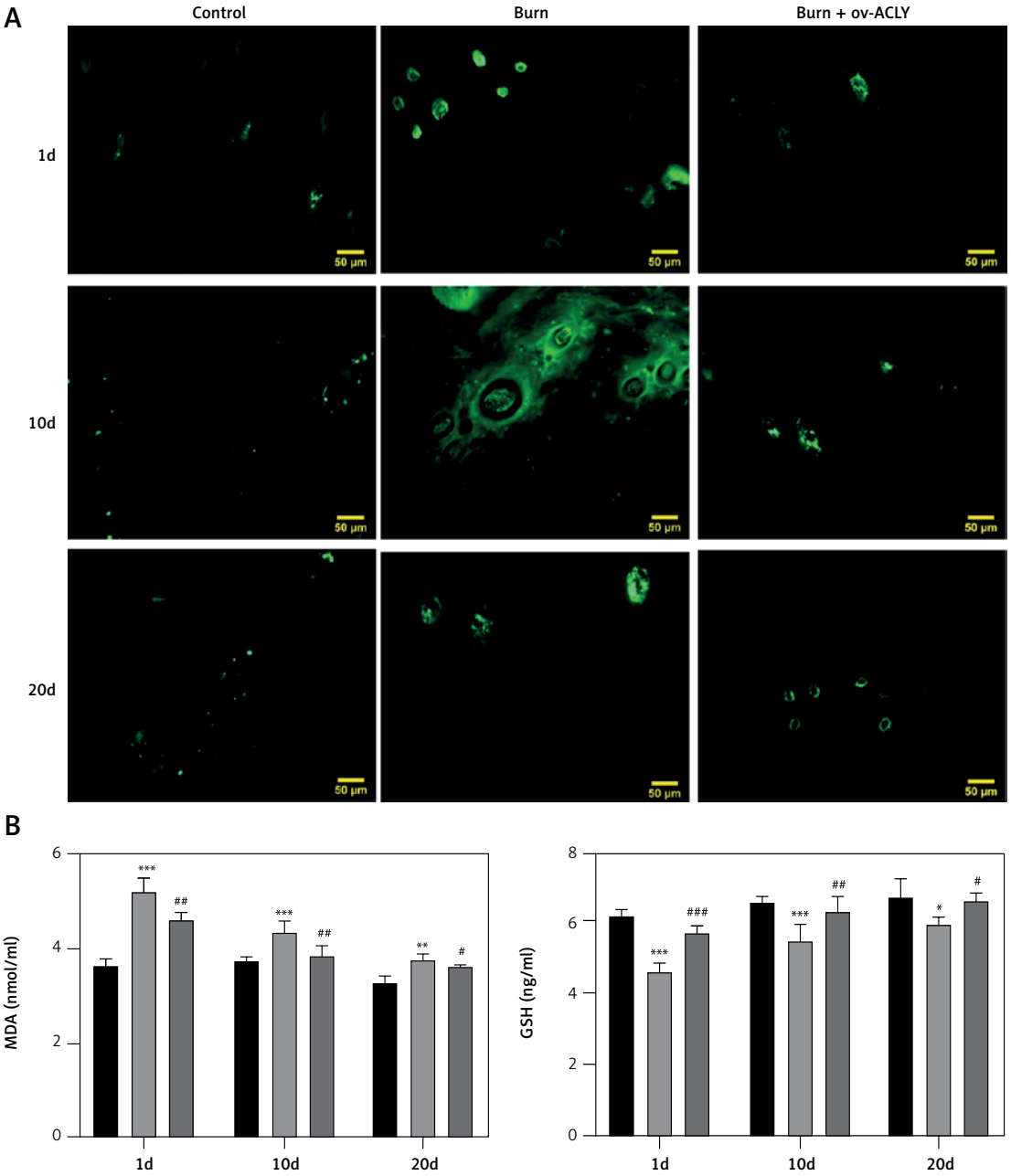

Figure 5. ACLY overexpression attenuates oxidative stress and mitochondrial dysfunction in burned skin tissues. **A** – DCFH-DA staining showing increased ROS accumulation in burned skin at days 1, 10, and 20 postinjury compared with control tissues. ACLY overexpression markedly reduced oxidative signals. **B** – Quantification of lipid peroxidation (MDA) and reduced glutathione (GSH) levels. Burn injury significantly elevated MDA and decreased GSH, whereas ACLY overexpression partially reversed these changes. Burn injury reduced fusion proteins (MFN1, MFN2, OPA1) and increased the fission marker DRP1. These changes were attenuated by ACLY overexpression. All data are presented as mean ± SD (n = 5, *p < 0.05, **p < 0.01, ***p < 0.001 vs. the control group; #p < 0.05, ##p < 0.01, ###p < 0.001 vs. the burn group). Statistical analysis was performed using two-way ANOVA followed by Tukey's multiple comparison test

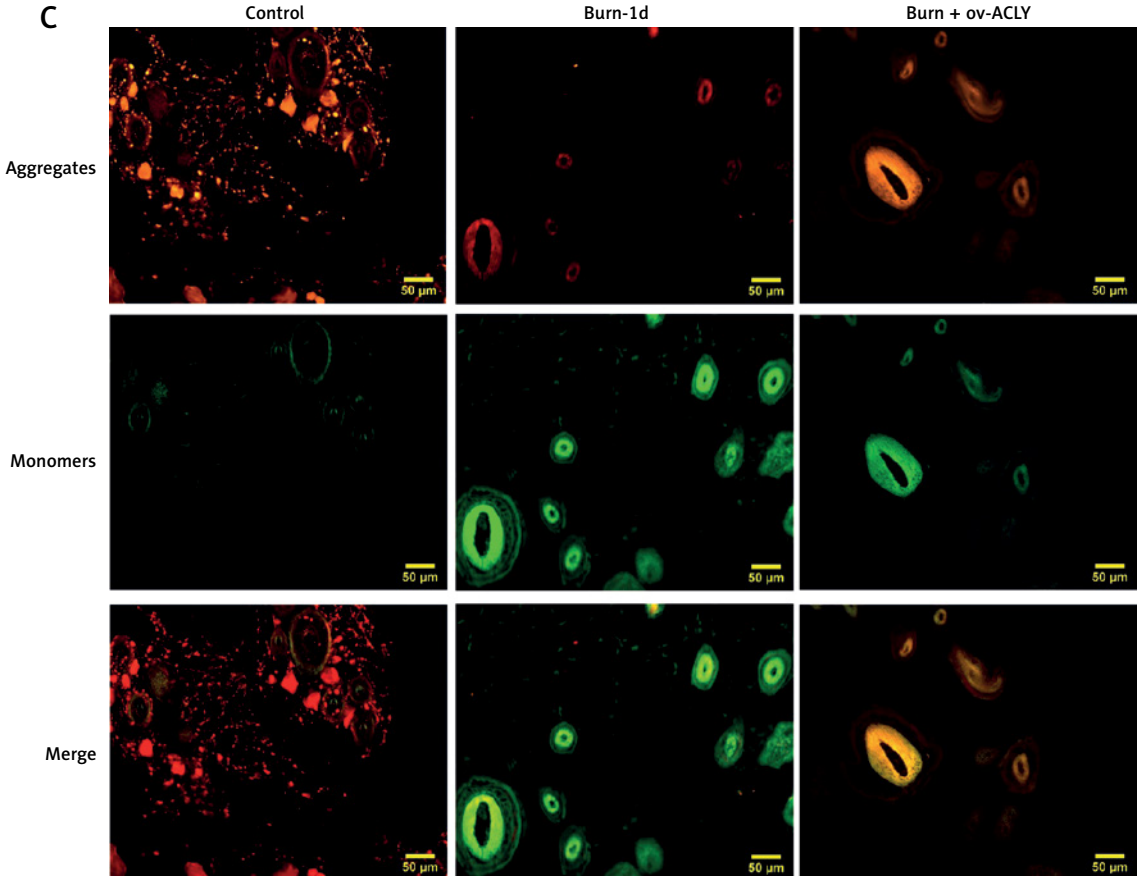

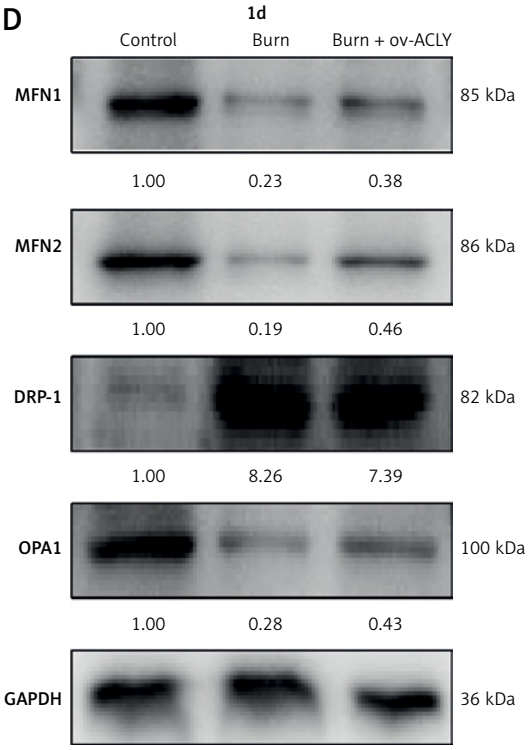

Figure 5. Cont. **C** – JC-1 staining at days 1 (**C**), 10 (**E**), and 20 (**G**) showing loss of mitochondrial membrane potential in burned tissues, as indicated by decreased red fluorescence (aggregates) and increased green fluorescence (monomers). ACLY overexpression attenuated the loss of $\Delta\Psi$m, as reflected by improved red/green fluorescence ratios. **D** – Western blot analysis of mitochondrial dynamics proteins at days 1 (**D**), 10 (**F**), and 20 (**H**). Burn injury reduced fusion proteins (MFN1, MFN2, OPA1) and increased the fission marker DRP1. These changes were attenuated by ACLY overexpression. All data are presented as mean ± SD (n = 5, $^{*}p < 0.05$, $^{**}p < 0.01$, $^{***}p < 0.001$ vs. the control group; $\#p < 0.05$, $\#\#p < 0.01$, $\#\#\#p < 0.001$ vs. the burn group). Statistical analysis was performed using two-way ANOVA followed by Tukey's multiple comparison test

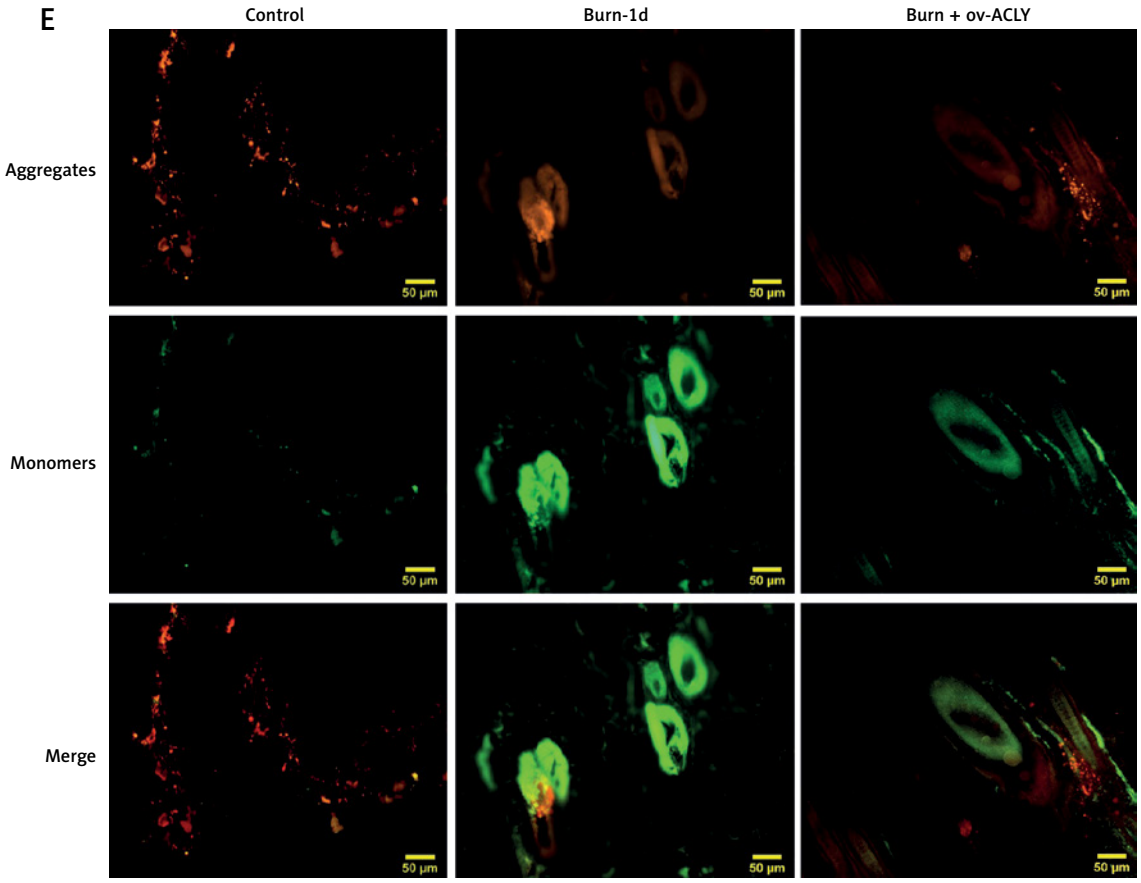

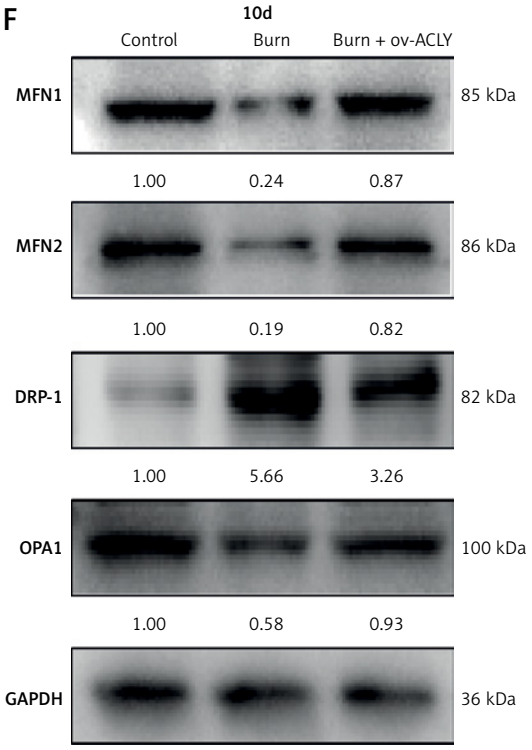

Figure 5. Cont. **E** – JC-1 staining at days 1 (**C**), 10 (**E**), and 20 (**G**) showing loss of mitochondrial membrane potential in burned tissues, as indicated by decreased red fluorescence (aggregates) and increased green fluorescence (monomers). ACLY overexpression attenuated the loss of $\Delta\Psi m$, as reflected by improved red/green fluorescence ratios. **F** – Western blot analysis of mitochondrial dynamics proteins at days 1 (**D**), 10 (**F**), and 20 (**H**). Burn injury reduced fusion proteins (MFN1, MFN2, OPA1) and increased the fission marker DRP1. These changes were attenuated by ACLY overexpression. All data are presented as mean ± SD (n = 5, $^{*}p < 0.05$, $^{**}p < 0.01$, $^{***}p < 0.001$ vs. the control group; $\#p < 0.05$, $\#\#p < 0.01$, $\#\#\#p < 0.001$ vs. the burn group). Statistical analysis was performed using two-way ANOVA followed by Tukey's multiple comparison test

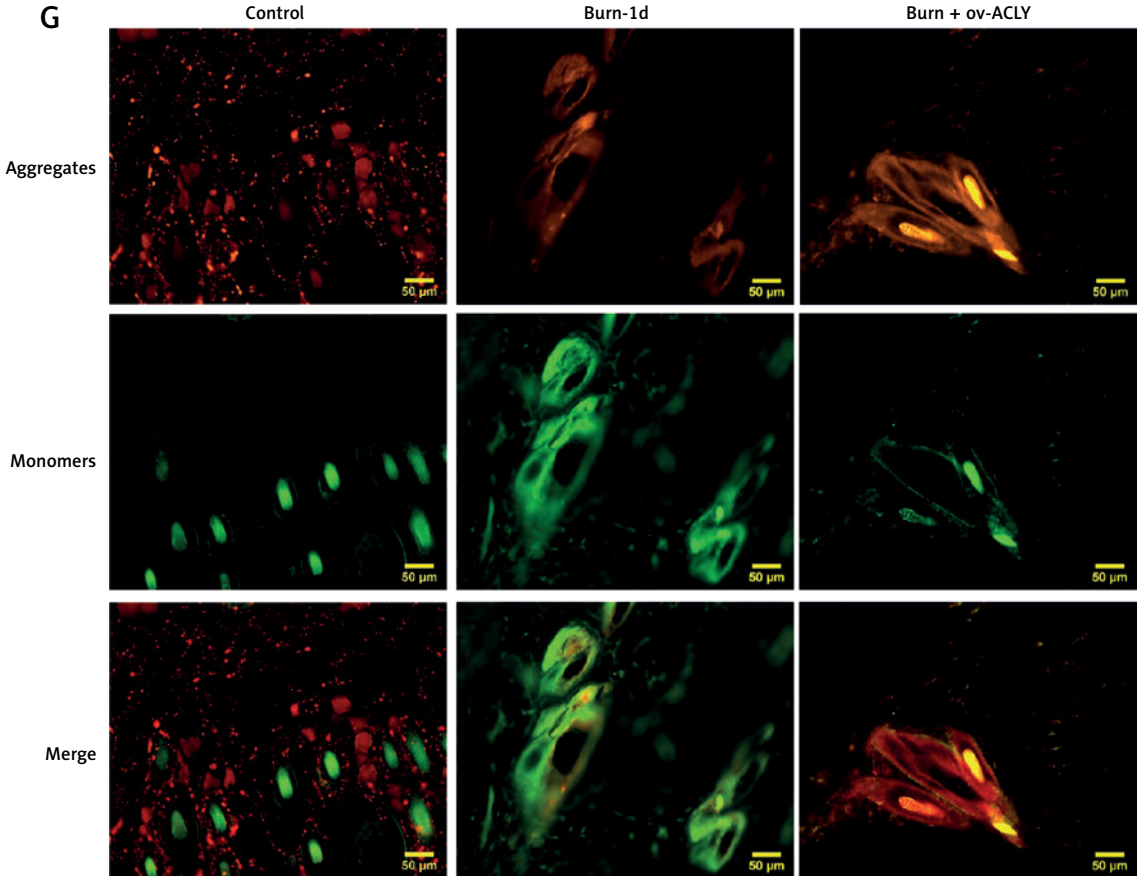

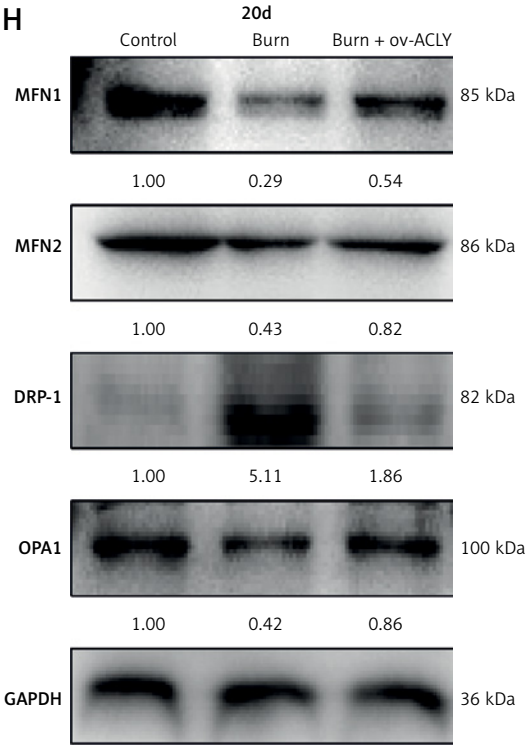

Figure 5. Cont. **G** – JC-1 staining at days 1 (**C**), 10 (**E**), and 20 (**G**) showing loss of mitochondrial membrane potential in burned tissues, as indicated by decreased red fluorescence (aggregates) and increased green fluorescence (monomers). ACLY overexpression attenuated the loss of $\Delta\Psi$m, as reflected by improved red/green fluorescence ratios. **H** – Western blot analysis of mitochondrial dynamics proteins at days 1 (**D**), 10 (**F**), and 20 (**H**). Burn injury reduced fusion proteins (MFN1, MFN2, OPA1) and increased the fission marker DRP1. These changes were attenuated by ACLY overexpression. All data are presented as mean ± SD (n = 5, $^{*}p < 0.05$, $^{**}p < 0.01$, $^{***}p < 0.001$ vs. the control group; $\#p < 0.05$, $\#\#p < 0.01$, $\#\#\#p < 0.001$ vs. the burn group). Statistical analysis was performed using two-way ANOVA followed by Tukey's multiple comparison test

evident at days 15 and 20 (Figure 6B). Histological analysis by HE staining demonstrated epidermal thickening, disorganized keratinocyte layers, and inflammatory infiltration in burn wounds (Figure 6C). Consistent with these findings, Western blot analysis showed that burn injury induced robust upregulation of IL-1β, IL-6, and TNFα at 1, 10, and 20 days post-injury, whereas ACLY overexpression reduced their expression across all time points (Figure 6D, F, H). Immunohistochemistry further revealed that IL-17 and IFN-γ were strongly expressed at wound edges in the burn group but significantly reduced by ACLY overexpression at days 1, 10, and 20 (Figure 6E, G).

Discussion

Burn injuries remain a major global health challenge, causing serious medical complications, mortality risks, and significant socioeconomic impacts [32, 33]. Despite progress in surgical methods, fluid management, and infection control [34], treatment outcomes remain unsatisfactory for severe burns [35]. The primary healing barrier stems from sustained disruption of the wound microenvironment, which is characterized by oxidative stress, impaired energy metabolism, chronic inflammation, and defective tissue regeneration [36, 37].

Mitochondrial impairment is a key factor in burn progression. After burns, cells show reduced mitochondrial biogenesis and function, collapsed membrane potential, and structural damage, all of which may contribute to increased ROS production and apoptosis [38, 39]. Heat-injured skin cells may develop membrane damage and mitochondrial dysfunction, activating cell death programs and slowing recovery [18, 40]. Existing treatments focus on closing wounds and supporting grafts, yet may not fully address cellular metabolic dysfunction during tissue repair [41]. Effective regeneration may require therapeutic strategies that revive energy output and protect cell architecture.

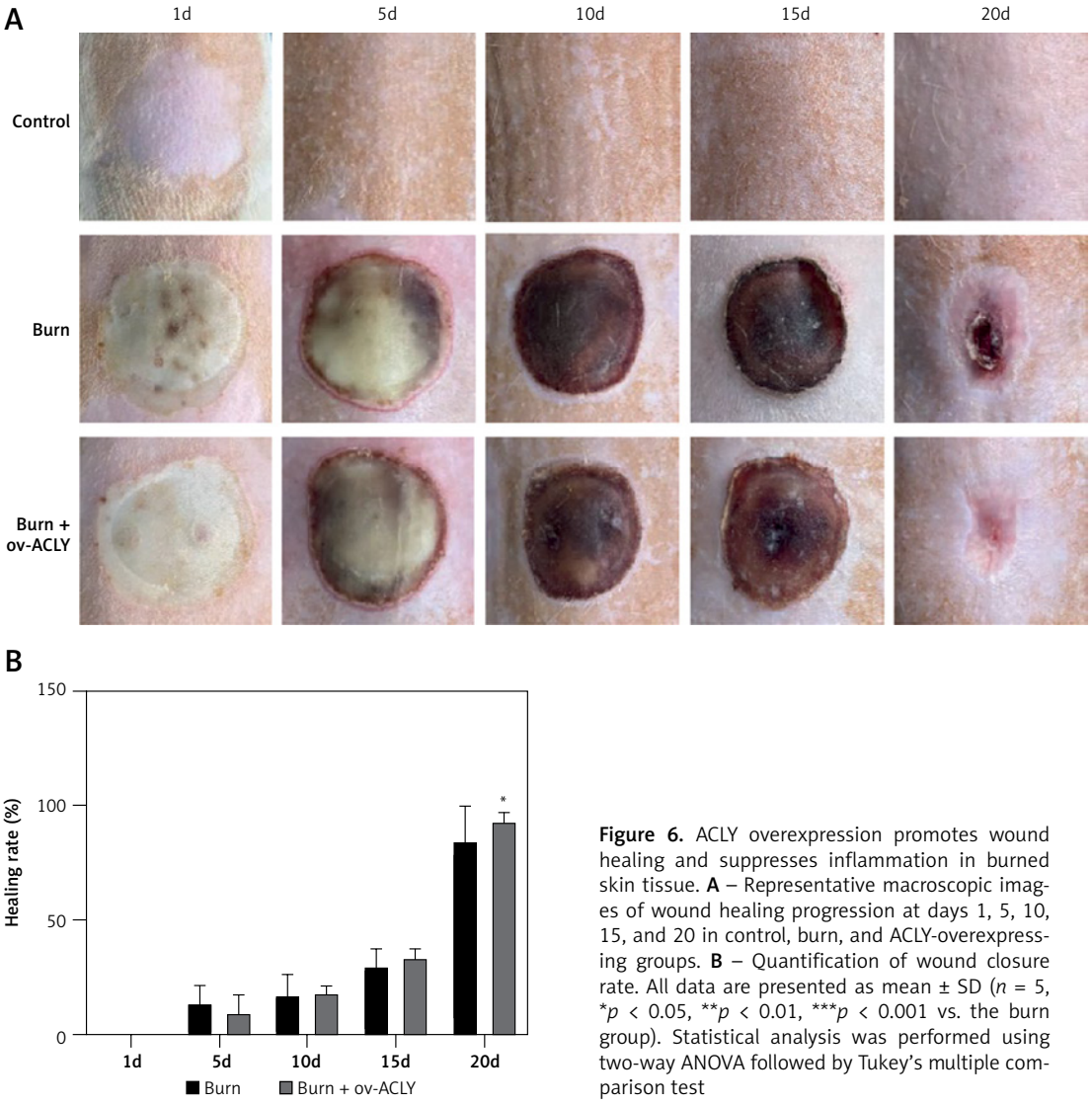

Figure 6. ACLY overexpression promotes wound healing and suppresses inflammation in burned skin tissue. **A** – Representative macroscopic images of wound healing progression at days 1, 5, 10, 15, and 20 in control, burn, and ACLY-overexpressing groups. **B** – Quantification of wound closure rate. All data are presented as mean ± SD (n = 5, *p < 0.05, **p < 0.01, ***p < 0.001 vs. the burn group). Statistical analysis was performed using two-way ANOVA followed by Tukey's multiple comparison test

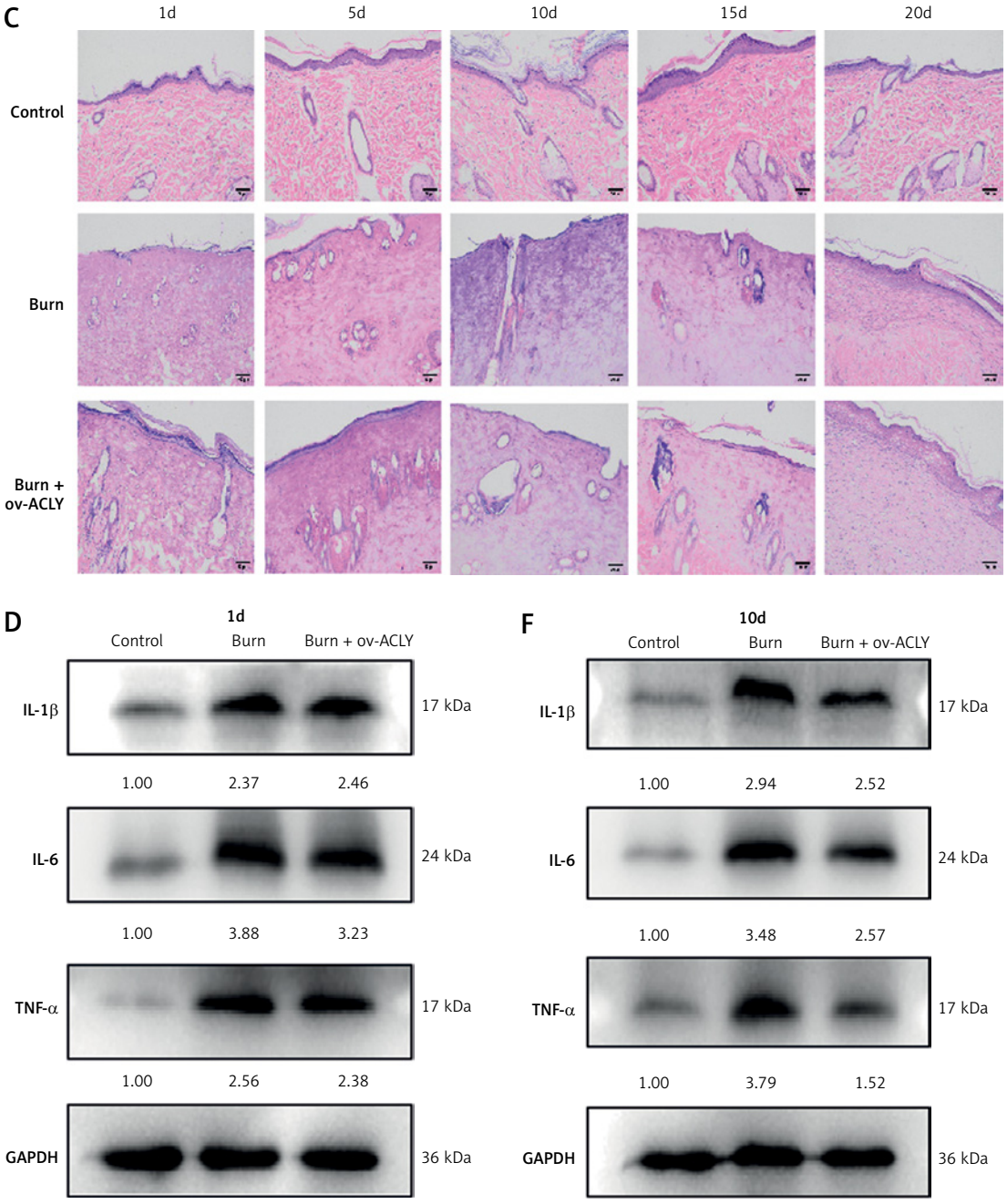

Figure 6. Cont. **C** – HE staining showing histological features of epidermal and dermal organization at different time points. **D**, **F** – Immunoblot analysis of IL-1β, IL-6, and TNF-α expression in control, burn, and ACLY-treated tissues at 1, 10, and 20 days post-injury. All data are presented as mean ± SD (n = 5, *p < 0.05, **p < 0.01, ***p < 0.001 vs. the burn group). Statistical analysis was performed using two-way ANOVA followed by Tukey's multiple comparison test

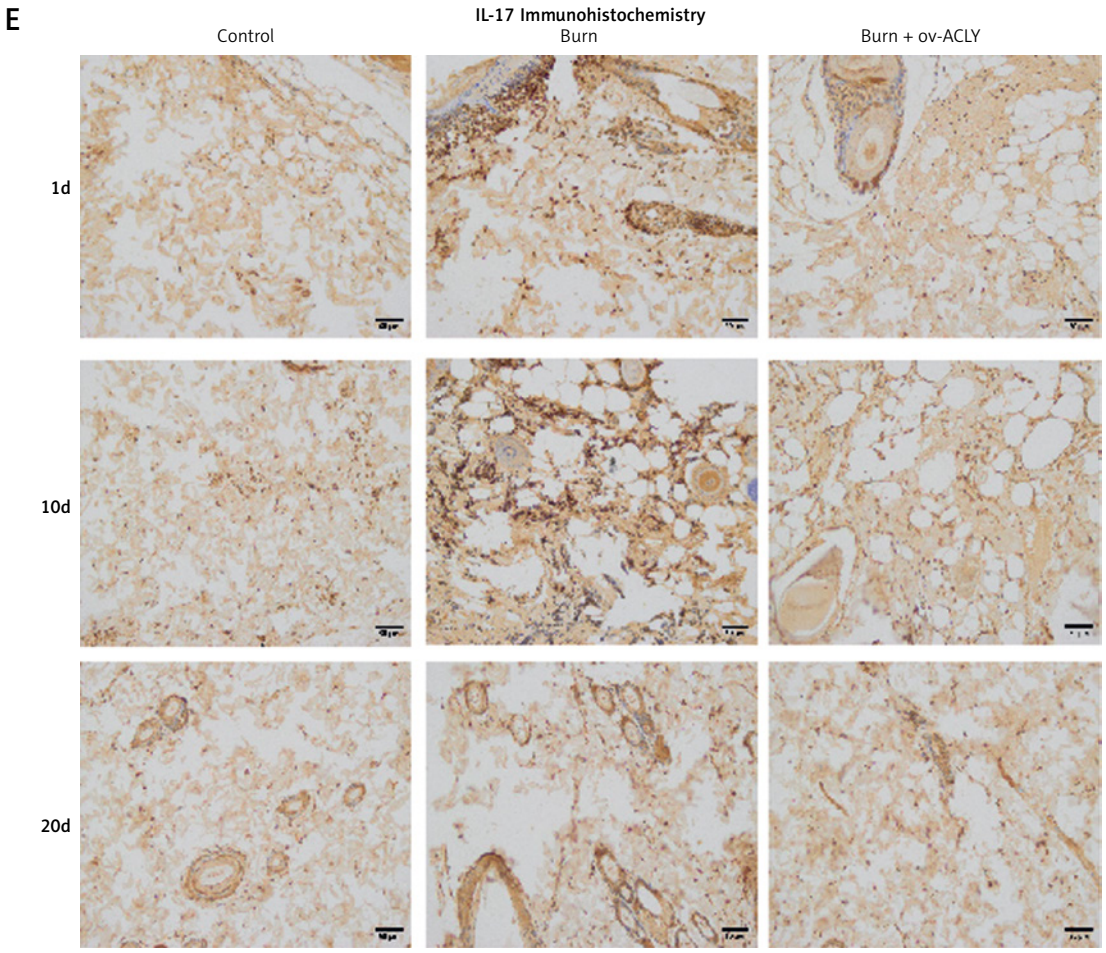

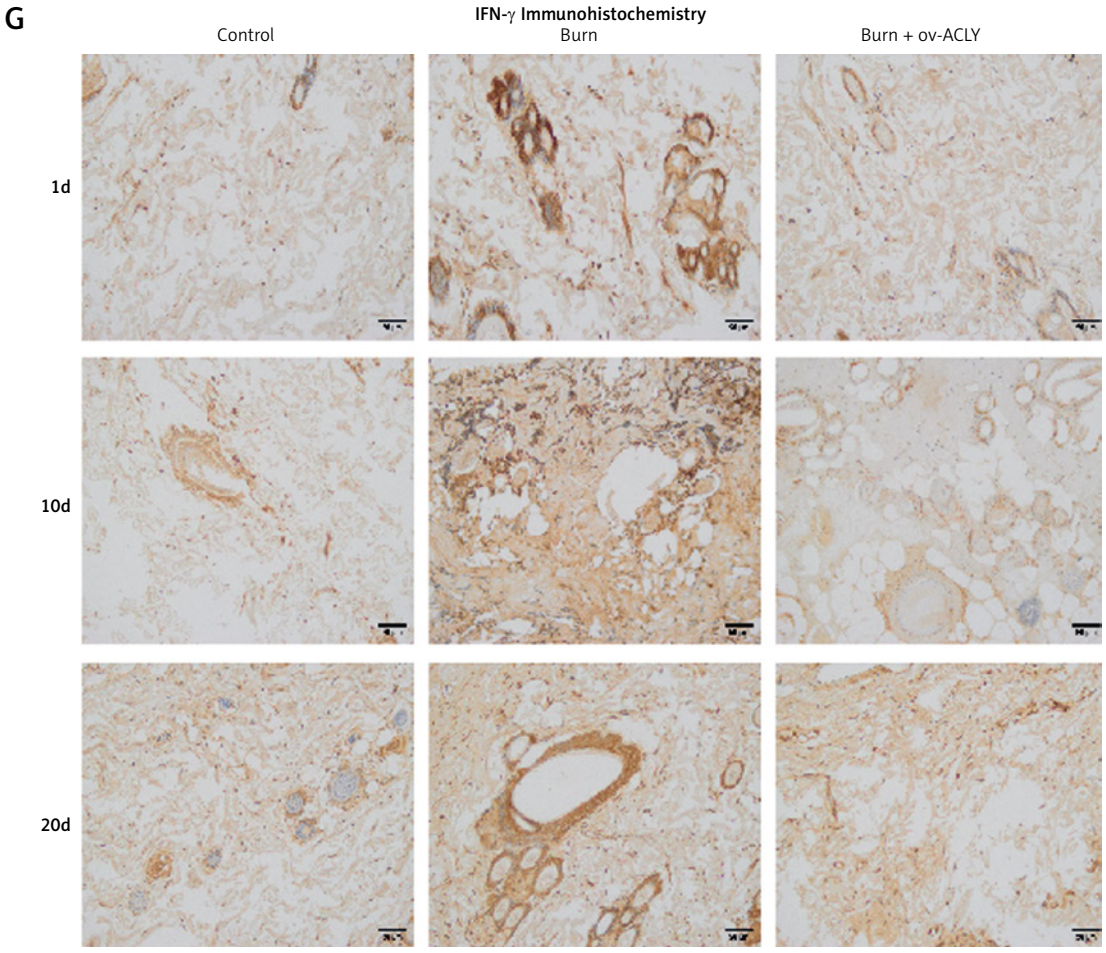

Figure 6. Cont. **E**, **G** – Immunohistochemical staining of IL-17 (**E**) and IFNγ (**G**) showing increased expression in burn wounds and attenuation following ACLY overexpression at days 1, 10, and 20. All data are presented as mean ± SD (n = 5, *p < 0.05, **p < 0.01, ***p < 0.001 vs. the burn group). Statistical analysis was performed using two-way ANOVA followed by Tukey's multiple comparison test

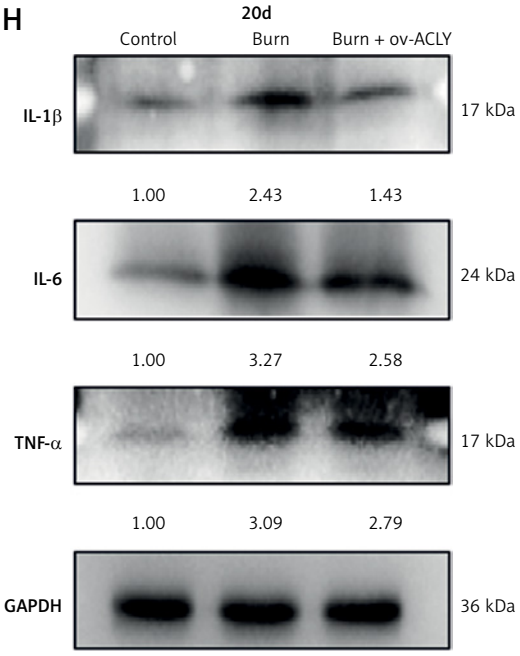

Figure 6. Cont. **H** – Immunoblot analysis of IL-1β, IL-6, and TNF-α expression in control, burn, and ACLY-treated tissues at 1, 10, and 20 days post-injury. All data are presented as mean ± SD (n = 5, *p < 0.05, **p < 0.01, ***p < 0.001 vs. the burn group). Statistical analysis was performed using two-way ANOVA followed by Tukey's multiple comparison test

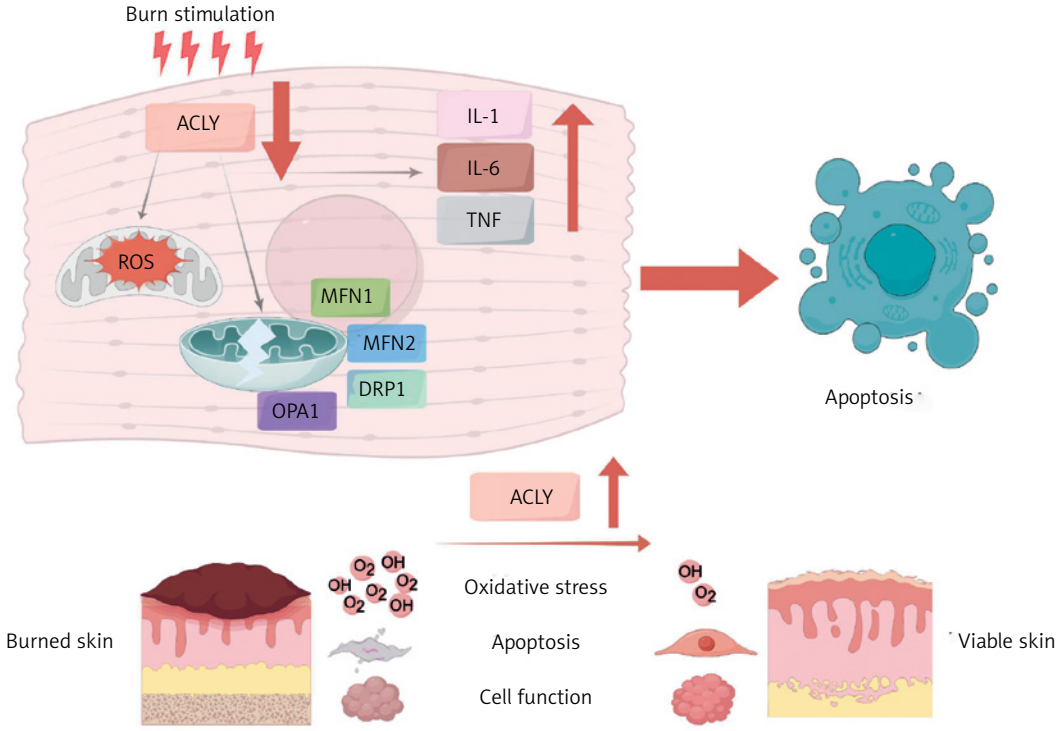

Figure 7. Schematic diagram illustrating the mechanism by which ACLY protects skin cells against burn injury. Burn stimulation downregulates ACLY expression, which is associated with excessive ROS production, mitochondrial dynamics imbalance (reduced expression of fusion proteins MFN1/2 and OPA1, increased expression of the fission protein DRP1), and elevated pro-inflammatory cytokines (IL-1, IL-6, TNF). These events collectively drive oxidative stress, inflammation, and cell apoptosis, leading to skin damage. In contrast, ACLY upregulation alleviates these pathological changes by mitigating oxidative stress, restoring mitochondrial homeostasis, reducing inflammation, and suppressing apoptosis, thereby promoting the recovery of viable skin tissue

Our findings suggest that reduced ACLY expression may contribute to impaired metabolic adaptation following burn injury, potentially affecting redox balance and mitochondrial function. Excess ROS accumulation can damage mitochondrial DNA and structure, creating a cycle of oxidative stress and cellular dysfunction. ROS accumulation may also activate apoptosis-related pathways, thereby exacerbating tissue injury. Thus, ACLY downregulation may represent one component of the metabolic stress response associated with burn-induced tissue damage. Halting this process could help overcome some limitations of current repair strategies. ACLY's role extends beyond metabolism to potential regulation of mitochondrial homeostasis, where it may influence proteins including MFN1, MFN2, OPA1, and DRP1. These proteins maintain mitochondrial fusion–fission balance, whose disruption leads to fragmentation and functional loss, increasing susceptibility to apoptosis. ACLY may also limit oxidative stress, supporting mitochondrial homeostasis and improving cell survival after burns [42]. Consistent with this protective role, our *in vivo* ACLY knockdown experiments further confirmed that loss of ACLY expression was associated with aggravated burn-induced mitochondrial dysfunction: ACLY deficiency further aggravated mitochondrial membrane potential depolarization, was accompanied by more severe mitochondrial fragmentation, and significantly amplified ROS accumulation and lipid peroxidation, while depleting cellular antioxidant reserves. These loss-of-function results complement our overexpression data, suggesting that ACLY contributes to the maintenance of mitochondrial integrity under thermal stress, and that its downregulation may directly accelerate the vicious cycle of oxidative stress and mitochondrial damage. However, the precise molecular mechanisms linking ACLY to mitochondrial dynamics require further investigation. ACLY-produced acetyl-CoA further supplies histone acetylation, bridging metabolic state and epigenetic gene regulation [43]. While not directly assessed in this work, earlier studies establish ACLY's ability to modify chromatin structure and transcription through acetylation [44]. This epigenetic link suggests a potential, though still unverified, path for ACLY to influence repair processes, requiring future validation.

In addition, ACLY-derived acetyl-CoA may serve as a pivotal link between metabolism and mitochondrial function [45, 46]. Beyond providing substrates for lipid synthesis, acetyl-CoA may contribute to membrane remodeling and mitochondrial homeostasis [47]. This morphological adaptation may support the maintenance of mitochondrial network integrity and energy production. The elevated energy supply may support key reparative events including keratinocyte proliferation and migration as well as fibroblast-driven collagen synthesis, thereby facilitating burn wound healing. Our findings are consistent with this mechanism and highlight a potential metabolic-mitochondrial axis involving ACLY in tissue repair.

Major burns cause severe immune disruption, starting with extreme inflammation that later shifts to immune suppression. This two-stage reaction raises the risk of infection and can lead to organ failure [48, 49]. Burn wounds exhibit excessive immune cell infiltration, prolonged inflammation, and impaired resolution [50], creating a damaging environment that hinders healing and promotes tissue damage [51]. Recent studies have identified mitochondrial molecules, including succinate and itaconate, as important immune regulators. These metabolites can influence phagocyte behavior and adjust inflammatory signals [52, 53]. A recent study showed that itaconate reprograms macrophages to reduce inflammation and promote wound repair [54]. Targeting mitochondrial-immune communication offers a promising treatment direction. Burns also reduce key antioxidants including glutathione and SOD, increasing oxidative harm and delaying recovery [55, 56]. Antioxidant therapies show limited clinical efficacy, likely due to poor delivery or incomplete metabolic correction [57]. Combined strategies targeting both oxidative stress and mitochondrial repair may prove more effective. Skin regeneration requires coordinated interactions among keratinocytes, fibroblasts, endothelial cells, and immune cells [58]. Modern genomic studies of burn wounds have revealed significant cellular diversity and stress-induced changes across skin, immune, and vascular cells [59, 60]. However, most studies still analyze cell types in isolation. Future studies should employ multicellular models or 3D tissue systems to better mimic actual wound healing processes. In our study, ACLY overexpression reduced pro-inflammatory cytokines (IL-1β, IL-6, TNF-α, IL-17, IFN-γ) in burned skin and stressed keratinocytes. While the exact mechanisms remain unclear, classical pathways such as NF-ᵋB, JAK/STAT, and NOTCH may be involved. ACLY could potentially influence these cascades through its metabolic-epigenetic functions, thereby attenuating inflammation [20, 61]. This possibility warrants further mechanistic validation.

This study revealed that the expression of ACLY in skin tissue was significantly downregulated after burn injury, and this change was associated with mitochondrial damage, inhibition of cell proliferation and migration, ROS accumulation, and increased apoptosis. These findings suggest that ACLY may represent an important metabolic regulator involved in the burn repair process through multiple biological mechanisms. Our study demonstrated the role of ACLY in maintain-

ing mitochondrial function and reducing oxidative stress, but important questions remain unanswered. The specific mechanisms regulating ACLY expression and activity after burn injury are still unknown. Possible regulators include hypoxia-related transcription factors, AMPK/mTOR metabolic pathways, and inflammatory signaling molecules. The specific biological pathways through which ACLY enhances tissue repair warrant further investigation: particularly its potential roles in epigenetic modification, fatty acid synthesis, and antioxidant defense systems. Therapeutically, genetic approaches demonstrate proof-of-concept but require further evaluation before translation into clinical applications. Small-molecule ACLY activators or nanoparticle-based delivery systems may represent potential therapeutic strategies, although their feasibility and safety remain to be established [62]. Chronic ACLY overexpression has cancer-promoting effects in some contexts [63], making accurate dosing and cell-specific delivery essential for therapeutic safety. Previous studies have focused on the regulation of glucose and lipids by ACLY in tumors and metabolic diseases, but this study suggests that ACLY downregulation is associated with multidimensional abnormalities in repair function in a burn model, expanding the pathophysiological significance of ACLY. Notably, the impact of ACLY on mitochondrial function may not occur in isolation; its ability to coordinate energy metabolism and biosynthesis through acetyl-CoA may distinguish ACLY from simple mitochondrial protective factors or antioxidant molecules. These findings provide a new perspective for understanding the potential interaction between metabolic regulation, cellular stress responses, and tissue repair in burn injury.

In addition to ACLY regulation, other metabolic regulators involved in wound healing have been identified in recent studies. Specifically, SIRT3 and CPT1A have been reported to promote mitochondrial regeneration and skin repair [64–66]. The balance between glycolysis and fatty acid oxidation may influence wound healing outcomes by affecting whether inflammation persists or tissue regeneration occurs [67, 68]. Collectively, our complementary loss-of-function studies further support this conclusion: ACLY knockdown *in vivo* aggravated several pathological features of burn injury, including increased tissue necrosis, delayed wound closure, enhanced apoptosis, suppressed proliferation, amplified inflammation, and worsened oxidative stress and mitochondrial dysfunction. These findings, together with our overexpression data, support a causal contribution of ACLY expression to burn repair outcomes and identify ACLY as an important regulator of thermal stress-induced skin injury. Future studies should investigate whether pharmacological modulation of ACLY activity can improve burn outcomes and evaluate its therapeutic potential in clinically relevant models. In conclusion, burn injury triggers a complex cascade of mitochondrial, oxidative, and immune dysfunctions that collectively impair skin regeneration. Future research should prioritize the identification of upstream signals, downstream effectors, and cell type-specific responses to metabolic stress in burn patients. A systems biology approach that incorporates transcriptomics, metabolomics, and advanced modelling may ultimately lead to more precise therapeutic interventions for burn patients.

This study identified ACLY as an important regulator of the response to thermal injury, reducing oxidative damage and improving mitochondrial homeostasis during burn repair. Increased ACLY expression improves keratinocyte functions, including proliferation, migration, and mitochondrial activity, collectively contributing to faster skin repair. ACLY appears to promote wound healing through multiple mechanisms, including attenuation of oxidative stress, improvement of mitochondrial integrity, and modulation of inflammatory responses (Figure 7). These findings highlight ACLY as a potential therapeutic target for improving burn wound healing and reducing tissue damage.

Funding

The research was supported by the Anhui Science and Technology Tackling Project (No. 1604a0802083 to Qinglian Xu) and the Educational Commission foundation of Anhui Province (No.2023AH040262 to Jianjun Qi).

Ethical approval

The study was approved by The First Affiliated Hospital of Wannan Medical University (Yijishan Hospital of Wannan Medical University), Wannan Medical University (approval number: WNMC-AWE-2024412).

Conflict of interest

The authors declare no conflict of interest.

References

1. Radzikowska-Büchner E, Łopuszyńska I, Flieger W, et al. An overview of recent developments in the management of burn injuries. Int J Mol Sci 2023; 24: 16357.
2. Dobson GP, Morris JL, Letson HL. Pathophysiology of severe burn injuries: new therapeutic opportunities from a systems perspective. J Burn Care Res 2024; 45: 1041-50.
3. Shah NR, Palackic A, Brondeel KC, et al. The burn wound. Surg Clin North Am 2023; 103: 453-62.
4. Palackic A, Duggan RP, Campbell MS, et al. The role of skin substitutes in acute burn and reconstructive burn

surgery: an updated comprehensive review. Semin Plast Surg 2022; 36: 33-42.
5. Huang S, Xie K, Li X, Xu X, Chen P. The role of the STING inflammatory pathway in hepatic damage in psoriasis with type 2 diabetes mellitus. Arch Med Sci 2024; 20: 1426-41.
6. Wang Z, Zhao F, Xu C, et al. Metabolic reprogramming in skin wound healing. Burns Trauma 2024; 12: tkad047.
7. Badoiu SC, Miricescu D, Stanescu-Spinu II, et al. Glucose metabolism in burns-what happens? Int J Mol Sci 2021; 22: 5159.
8. Li HH, Zhou XM, Liu T, et al. The clinical value of metagenomic next-generation sequencing for rapid microbial identification of chronic granulation wound infections. Arch Med Sci 2023; 19: 1162-7.
9. Clark A, Imran J, Madni T, Wolf SE. Nutrition and metabolism in burn patients. Burns Trauma 2017; 5: 11.
10. Asuku M, Shupp JW. Burn wound conversion: clinical implications for the treatment of severe burns. J Wound Care 2023; 32 (Suppl. 5): S11-20.
11. Pratap A, Monge KM, Qualman AC, Kovacs EJ, Idrovo JP. Burn-induced mitochondrial dysfunction in hepatocytes: The role of methylation-controlled J protein silencing. J Trauma Acute Care Surg 2025; 98: 204-11.
12. Harrington JS, Ryter SW, Plataki M, Price DR, Choi AMK. Mitochondria in health, disease, and aging. Physiol Rev 2023; 103: 2349-422.
13. Vringer E, Tait SWG. Mitochondria and cell death-associated inflammation. Cell Death Differ 2023; 30: 304-12.
14. Al Amir Dache Z, Thierry AR. Mitochondria-derived cell-to-cell communication. Cell Rep 2023; 42: 112728.
15. Palma FR, Gantner BN, Sakiyama MJ, et al. ROS production by mitochondria: function or dysfunction? Oncogene 2024; 43: 295-303.
16. Piipponen M, Li D, Landén NX. The immune functions of keratinocytes in skin wound healing. Int J Mol Sci 2020; 21: 8790.
17. Rennekampff HO, Alharbi Z. Burn injury: mechanisms of keratinocyte cell death. Med Sci (Basel) 2021; 9: 51.
18. Prabhakaran HS, Hu D, He W, Luo G, Liou YC. Mitochondrial dysfunction and mitophagy: crucial players in burn trauma and wound healing. Burns Trauma 2023; 11: tkad029.
19. Liu Y, Birsoy K. Metabolic sensing and control in mitochondria. Mol Cell 2023; 83: 877-89.
20. Dominguez M, Brüne B, Namgaladze D. Exploring the role of ATP-citrate lyase in the immune system. Front Immunol 2021; 12: 632526.
21. Korobkina ED, Martinez Calejman C, Haley JA, et al. Brown fat ATP-citrate lyase links carbohydrate availability to thermogenesis and guards against metabolic stress. Nat Metab 2024; 6: 2187-202.
22. Convertini P, Santarsiero A, Todisco S, et al. ACLY as a modulator of liver cell functions and its role in metabolic dysfunction-associated steatohepatitis. J Transl Med 2023; 21: 568.
23. Li W, Han J, Huang B, et al. SLC25A1 and ACLY maintain cytosolic acetyl-CoA and regulate ferroptosis susceptibility via FSP1 acetylation. EMBO J 2025; 44: 1641-62.
24. Chen Q, Du J, Cui K, et al. Acetyl-CoA derived from hepatic mitochondrial fatty acid β-oxidation aggravates inflammation by enhancing p65 acetylation. iScience 2021; 24: 103244.
25. Pay SL, Qi X, Willard JF, et al. Improving the transduction of bone marrow-derived cells with an integrase-defective lentiviral vector. Hum Gene Ther Methods 2017; 29: 44-59.
26. Cai EZ, Ang CH, Raju A, et al. Creation of consistent burn wounds: a rat model. Arch Plast Surg 2014; 41: 317-24.
27. Singer AJ, Wang E, Taira BR, Steinhauff N, Rooney J, Zimmerman T. Controlled mild hypothermia prolongs survival in a rat model of large scald burns. Acad Emerg Med 2011; 18: 287-91.
28. Davenport L, Dobson G, Letson H. A new model for standardising and treating thermal injury in the rat. MethodsX 2019; 6: 2021-7.
29. Xu Z, Zhu X, Mu S, et al. FTO overexpression expedites wound healing and alleviates depression in burn rats through facilitating keratinocyte migration and angiogenesis via mediating TFPI-2 demethylation. Mol Cell Biochem 2024; 479: 325-35.
30. Pourfath MR, Behzad-Behbahani A, Hashemi SS, Derakhsahnfar A, Taheri MN, Salehi S. Monitoring wound healing of burn in rat model using human Wharton's jelly mesenchymal stem cells containing cGFP integrated by lentiviral vectors. Iran J Basic Med Sci 2018; 21: 70-6.
31. Livak KJ, Schmittgen TD. Analysis of relative gene expression data using real-time quantitative PCR and the 2(-Delta Delta C(T)) method. Methods 2001; 25: 402-8.
32. Haruta A, Mandell SP. Assessment and management of acute burn injuries. Phys Med Rehabil Clin N Am 2023; 34: 701-16.
33. Sengul T, Kirkland-Kyhn H, Gul A. Postacute overview of burn injuries: pathophysiology, management, and future directions. Nurs Clin North Am 2025; 60: 15-25.
34. Rex S. Burn injuries. Curr Opin Crit Care 2012; 18: 671-6.
35. Kiley JL, Greenhalgh DG. Infections in burn patients. Surg Clin North Am 2023; 103: 427-37.
36. Kirchner S, Lei V, MacLeod AS. The cutaneous wound innate immunological microenvironment. Int J Mol Sci 2020; 21: 8748.
37. Alharbi MA, Shahlol AMA, Albureikan MOI, et al. Investigating the multi-targeted pharmacological profile of an exopolysaccharide from Bacillus rugosus SYG20 via in vitro evaluation of its antioxidant, anti-inflammatory, antidiabetic, wound healing, and antimicrobial properties. Arch Med Sci 2025; 21: 2389-405.
38. Li Q, Song H, Li S, et al. Macrophage metabolism reprogramming EGCG-Cu coordination capsules delivered in polyzwitterionic hydrogel for burn wound healing and regeneration. Bioact Mater 2023; 29: 251-64.
39. Feng J, Thangaveloo M, Ong YS, Chong SJ, Joethy YV, Becker DL. Connexin 43 upregulation in burns promotes burn conversion through spread of apoptotic death signals. Burns 2020; 46: 1389-97.
40. Liu Z, Bian X, Luo L, et al. Spatiotemporal single-cell roadmap of human skin wound healing. Cell Stem Cell 2025; 32: 479-98.e8.
41. Ashouri S. An introduction to burns. Phys Med Rehabil Clin N Am 2022; 33: 871-83.
42. Hu C, Xin Z, Sun X, et al. Activation of ACLY by SEC63 deploys metabolic reprogramming to facilitate hepatocellular carcinoma metastasis upon endoplasmic reticulum stress. J Exp Clin Cancer Res 2023; 42: 108.
43. Wellen KE, Hatzivassiliou G, Sachdeva UM, Bui TV, Cross JR, Thompson CB. ATP-citrate lyase links cellular metabolism to histone acetylation. Science 2009; 324: 1076-80.
44. Nitsch S, Zorro Shahidian L, Schneider R. Histone acylations and chromatin dynamics: concepts, challenges, and links to metabolism. EMBO Rep 2021; 22: e52774.
45. Nguyen PTT, Shiue M, Kuprasertkul N, et al. Acetyl-CoA synthesis in the skin is a key determinant of systemic lipid homeostasis. Cell Rep 2025; 44: 115284.

46. Izzo LT, Trefely S, Demetriadou C, et al. Acetylcarnitine shuttling links mitochondrial metabolism to histone acetylation and lipogenesis. Sci Adv 2023; 9: eadf0115.
47. Puccini J, Wei J, Tong L, Bar-Sagi D. Cytoskeletal association of ATP citrate lyase controls the mechanodynamics of macropinocytosis. Proc Natl Acad Sci USA 2023; 120: e2213272120.
48. Gibson BHY, Wollenman CC, Moore-Lotridge SN, et al. Plasmin drives burn-induced systemic inflammatory response syndrome. JCI Insight 2021; 6: e154439.
49. Prudovsky I, Kacer D, Lindner V, Rappold J, Carter DW. Tranexamic acid reduces inflammation, edema and burn wound conversion in a rodent model. Burns 2024; 50: 947-56.
50. AlHawaj A, lMadhoob M, Alkhanaizi R, AlHaddad A. Evaluation of white blood cell count, lymphocyte percentage, neutrophil percentage, and elevated temperature as predictors of wound infection in burn patients. Cureus 2024; 16: e63172.
51. Wu LJ, Lin W, Liu JJ, et al. Transplantation of human induced pluripotent stem cell derived keratinocytes accelerates deep second-degree burn wound healing. World J Stem Cells 2023; 15: 713-33.
52. Lampropoulou V, Sergushichev A, Bambouskova M, et al. Itaconate links inhibition of succinate dehydrogenase with macrophage metabolic remodeling and regulation of inflammation. Cell Metab 2016; 24: 158-66.
53. Mills EL, Kelly B, Logan A, et al. Succinate dehydrogenase supports metabolic repurposing of mitochondria to drive inflammatory macrophages. Cell 2016; 167: 457-70.e13.
54. Maassen S, Coenen B, Ioannidis M, et al. Itaconate promotes a wound resolving phenotype in pro-inflammatory macrophages. Redox Biol 2023; 59: 102591.
55. Claeyssen R, Andriollo-Sanchez M, Arnaud J, et al. Burn-induced oxidative stress is altered by a low zinc status: kinetic study in burned rats fed a low zinc diet. Biol Trace Elem Res 2008; 126 Suppl. 1: S80-96.
56. Horton JW. Free radicals and lipid peroxidation mediated injury in burn trauma: the role of antioxidant therapy. Toxicology 2003; 189: 75-88.
57. Raposio E, Grieco MP, Caleffi E. Evaluation of plasma oxidative stress, with or without antioxidant supplementation, in superficial partial thickness burn patients: a pilot study. J Plast Surg Hand Surg 2017; 51: 393-8.
58. Sriram G, Bigliardi PL, Bigliardi-Qi M. Fibroblast heterogeneity and its implications for engineering organotypic skin models in vitro. Eur J Cell Biol 2015; 94: 483-512.
59. Huang J, Zhu Z, Ji D, et al. Single-cell transcriptome profiling reveals neutrophil heterogeneity and functional multiplicity in the early stage of severe burn patients. Front Immunol 2021; 12: 792122.
60. Cheng XC, Tong WZ, Rui W, Feng Z, Shuai H, Zhe W. Single-cell sequencing technology in skin wound healing. Burns Trauma 2024; 12: tkae043.
61. Santarsiero A, Convertini P, Todisco S, et al. ACLY nuclear translocation in human macrophages drives proinflammatory gene expression by NF-ᵌB acetylation. Cells 2021; 10: 2969.
62. Yu L, Zhou X, Liu Z, et al. Carrier-free nanoagent interfering with cancer-associated fibroblasts' metabolism to promote tumor penetration for boosted chemotherapy. Nano Lett 2024; 24: 11976-84.
63. Lucenay KS, Doostan I, Karakas C, et al. Cyclin E associates with the lipogenic enzyme ATP-citrate lyase to enable malignant growth of breast cancer cells. Cancer Res 2016; 76: 2406-18.
64. Su S, Ndiaye M, Singh CK, Ahmad N. Mitochondrial sirtuins in skin and skin cancers. Photochem Photobiol 2020; 96: 973-80.
65. Liu X, Xie X, Li D, et al. Sirt3-dependent regulation of mitochondrial oxidative stress and apoptosis contributes to the dysfunction of pancreatic islets after severe burns. Free Radic Biol Med 2023; 198: 59-67.
66. Su J, Liu J, Yan XY, et al. Cytoprotective effect of the UCP2-SIRT3 signaling pathway by decreasing mitochondrial oxidative stress on cerebral ischemia-reperfusion injury. Int J Mol Sci 2017; 18: 1599.
67. Manchanda M, Torres M, Inuossa F, et al. Metabolic reprogramming and reliance in human skin wound healing. J Invest Dermatol 2023; 143: 2039-51.e10.
68. Kusumo MHB, Prayitno A, Soetrisno, Laqif A. Synergistic therapeutic approach for hemorrhoids: integrating mesenchymal stem cells with diosmin-hesperidin to target tissue edema and inflammation. Arch Med Sci 2024; 20: 1556-66.